

1 A high-Arctic inner shelf–fjord system from the Last Glacial
2 Maximum to the Present: Bessel Fjord and SW Dove Bugt, NE
3 Greenland

4 Authors: Kevin Zoller¹; Jan Sverre Laberg¹; Tom Arne Rydningen¹, Katrine Husum² & Matthias
5 Forwick¹

6 ¹Department of Geosciences, UiT The Arctic University of Norway, Box 6050 Langnes, NO-
7 9037 Tromsø, Norway ²Norwegian Polar Institute, Box 6606 Langnes, NO-9296 Tromsø,
8 Norway

9 *Correspondence to:* Kevin Zoller (kevin.zoller3@gmail.com)

10 **Abstract**

11 The Greenland Ice Sheet (GrIS) responds rapidly to the present climate, therefore, its response
12 to the predicted future warming is of concern. To learn more about the impact of future climatic
13 warming on the ice sheet, decoding its behavior during past periods of warmer than present
14 climate is important. However, due to the scarcity of marine studies reconstructing ice sheet
15 conditions on the Northeast Greenland shelf and adjacent fjords, the timing of the deglaciation
16 over marine regions and its connection to forcing factors remain poorly constrained. This
17 includes data collected in fjords that encompass the Holocene Thermal Maximum (HTM), a
18 period in which the climate was warmer than it is at present. This paper aims to use bathymetric
19 data and the analysis of sediment gravity cores to enhance our understanding of ice dynamics
20 of the GrIS in a fjord and inner shelf environment as well as give insight into the timing of
21 deglaciation and provide a palaeoenvironmental reconstruction of southwestern Dove Bugt and
22 Bessel Fjord since the Last Glacial Maximum (LGM). The swath bathymetry data displayed in
23 this study is the first time the bathymetry for Bessel Fjord has become available. North-south
24 oriented glacial lineations, and the absence of pronounced moraines in southwest Dove Bugt,
25 an inner continental shelf embayment (trough), suggests the southwards and offshore flow of
26 the southern branch of the Northeast Greenland Ice Stream (NEGIS), Storstrømmen.
27 Sedimentological data suggests that an ice body, theorized to be the NEGIS, may have
28 retreated from the region slightly before ~11.4 ka cal BP. The seabed morphology of Bessel
29 Fjord, a fjord terminating in southern Dove Bugt, includes numerous basins, separated by
30 thresholds. The position of basin thresholds, which include some recessional moraines, suggest
31 that the GrIS had undergone multiple halts or readvances during deglaciation, likely during one
32 of the cold events identified in the Greenland Summit temperature records (Kobashi et al.,
33 2017). A minimum age of 7.1 ka cal BP is proposed for the retreat of ice through the fjord to or
34 west of its present-day position in the Bessel Fjord catchment area. This suggests that the GrIS
35 retreated from the marine realm in early Holocene, around the onset of the Holocene Thermal
36 Maximum in this region, a period when the mean July temperature according to Bennike et al.,
37 (2008) was at least 2-3 °C higher than at present, and remained at or west of this onshore
38 position for the remainder of the Holocene. The transition from predominantly mud to muddy
39 sand layers in a mid-fjord core at ~4 ka cal BP may be the result of increased sediment input
40 from nearby and growing ice caps. This shift may suggest that in the late Holocene
41 (Meghalayan), a period characterized by a temperature drop to modern values, ice caps in
42 Bessel Fjord fluctuated with greater sensitivity to climatic conditions than the NE sector of the
43 GrIS.

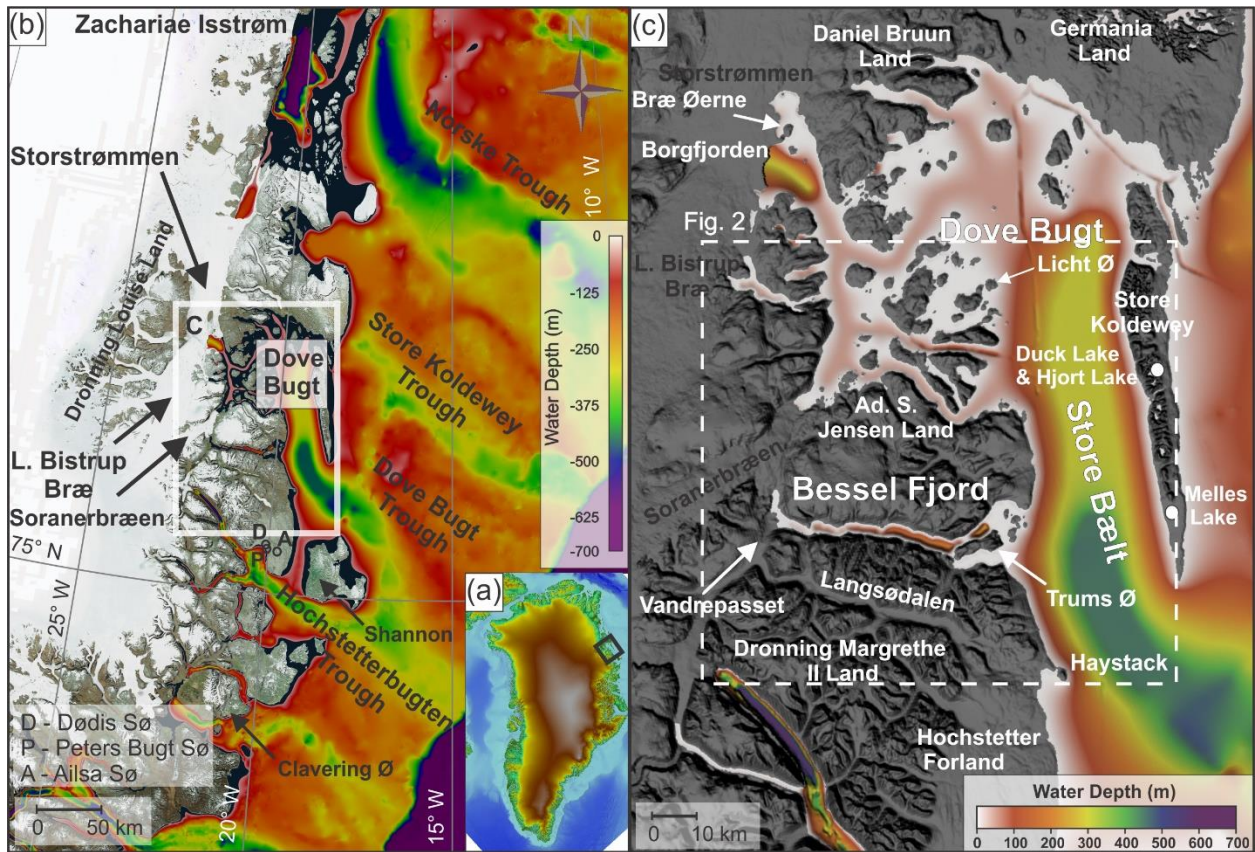
44 **1. Introduction**

45 Ice mass loss from the Greenland Ice Sheet (GrIS) has accelerated during the 21 century,
46 making it the largest individual contributor to sea level rise (King et al., 2020). This introduction
47 of a substantial quantity of fresh water may have ramifications for global ocean circulations as
48 well as the climate (Rahmstorf et al., 2015). Approximately 12% of the ice from the GrIS is
49 transported to the coast through the Northeast Greenland Ice Stream (NEGIS) (Khan et al.,
50 2014; Joughin et al., 2001) and therefore has a substantial impact on the mass balance of the
51 ice sheet and a potential to contribute to sea level rise. Currently, two of the three marine
52 terminating outlet glaciers that are supplied by the NEGIS are in retreat (Mouginot et al., 2015),
53 where the southernmost branch, Storstrømmen in Dove Bugt (Figs. 1a & 1b), is currently in a
54 building phase following a 1978-1984 surge (Khan et al., 2014; Reeh et al., 1994). While there
55 are numerous modern studies on the current state of the NEGIS during the past decades to
56 century, there is a scarcity of data concerning the position and dynamics of the ice stream, and
57 other local Northeast Greenland outlet glaciers, on a multi-century to millennia scale over
58 marine regions. Considering that the global mean temperature is expected to continue to rise
59 (Stocker et al., 2013), and that the Arctic will experience an amplification effect (Cohen et al.,
60 2014), looking to the past, especially during warmer than present periods (i.e., the Holocene
61 Thermal Maximum (HTM)), may provide an important insight into the future behavior of the ice
62 sheet.

63 Marine studies have found evidence for past advancement and retreat of the GrIS and NEGIS
64 along the continental shelf offshore Northeast Greenland (Evans et al., 2009; Winkelmann et al.,
65 2010; Arndt et al., 2015, 2017; Laberg et al., 2017; Arndt, 2018; Olsen et al., 2020; Syring et al.,
66 2020; Davies et al., 2022; Hansen et al., 2022; Jackson et al., 2022). Geomorphological findings
67 in Store Koldewey Trough (~76°N), a major shelf trough northeast of the study area (Fig. 1b),
68 suggests that the ice sheet may have reached the shelf break in this area during the LGM (Last
69 Glacial Maximum) (Laberg et al., 2017; Olsen et al., 2020). Further north (~79.4°N), the shelf
70 break is interpreted as being ice free during the LGM (Rasmussen et al., 2022), an area where
71 the ice front had its maximum LGM position at the outer shelf according to Arndt et al. (2017). A
72 concise understanding of the timing and dynamics of the ice sheet over the NE Greenland shelf
73 during the subsequent deglaciation of the marine realm remains to be established as very few
74 dated cores have been recovered. Terrestrial dating (e.g., cosmogenic nuclide dates and lake
75 studies) has provided further insight into when terrestrial regions had become deglaciated, and
76 how the climate has changed in these areas (e.g., Björck and Persson, 1981; Björck et al.,
77 1994; Wagner et al., 2008; Klug et al., 2009a; Schmidt et al., 2011; Briner et al., 2016; Skov et
78 al., 2020; Larsen et al., 2020). However, only recently has terrestrial data been integrated with
79 marine data to establish a detailed deglaciation chronology of the shelf, coastal and fjord
80 regions (Davies et al., 2022; Larsen et al., 2022).

81 Swath bathymetry and gravity cores data from southwestern Dove Bugt (i.e., Store Bælt) and
82 Bessel Fjord (Fig. 1), presented for the first time in this study, has been used to further refine
83 our understanding of how the GrIS responded to changes in palaeoclimatic conditions from the
84 LGM through the Holocene, including the HTM. Through this analysis we aim to reconstruct
85 regional ice dynamics from both full-glacial conditions and during overall retreat and put our
86 findings into the larger context of the dynamics of the Northeast Greenland Ice Sheet during
87 these periods. Additionally, this study aims to refine our understanding about the timing of
88 deglaciation over marine areas and compare findings to nearby terrestrial regions including the

89 Store Koldewey island and Hochstetter Forland/Shannon Ø. Results will also contribute to our
 90 understanding of palaeoenvironmental conditions throughout the Holocene for the NE
 91 Greenland fjords and inner shelf areas.



92
 93 *Figure 1. (a) An image of Greenland, using IBCAO 4.0 400x400m (Jakobsson et al., 2020), with a black box*
 94 *surrounding the study area. (b) Bathymetry of Northeast Greenland displayed using IBCAO 4.0 200x200m data*
 95 *(Jakobsson et al., 2020) and land is displayed using a World Imagery satellite image (Earthstar Geographics, Esri,*
 96 *HERE, Garmin, FAO, NOAA, USGS) made available through GlobalMapper. The white box surrounds the position of*
 97 *Fig. 1c. (c) Bathymetry of Dove Bugt and Bessel Fjord and surrounding land areas displayed using the IBCAO 4.0*
 98 *200x200m data (Jakobsson et al., 2020). Locations mentioned in the text are labelled here. The position of Fig. 2 is*
 99 *within the white dashed box.*

100 2. Regional Setting and Environmental History

101 Bessel Fjord is a west-east running fjord between Adolf S. Jensen Land and Dronning
 102 Margrethe II Land (Fig. 1c). The western end of the fjord contains the southern outlet glacier
 103 Soranerbræen, which also has a second outlet to the north in a tributary fjord to inner Dove Bugt
 104 (Fig. 2). Several ice caps are positioned across the length of the fjord (Figs. 2 & 3), some of
 105 which have several generations of moraines and glaciofluvial outlets that enter the fjord.
 106 Colluvial fans and rivers have been observed across the length of the fjord in satellite images
 107 and while surveying the fjord. Multiple islands are located at the entrance of Bessel Fjord, the
 108 largest of which, Trums Ø, splits the entrance into two main inlets (Figs. 1c & 2). From the
 109 termination of Soranerbræen to the entrance of the fjord measures ~60 km in length. The width
 110 of the fjord ranges from 1.8 to 3.7 km.

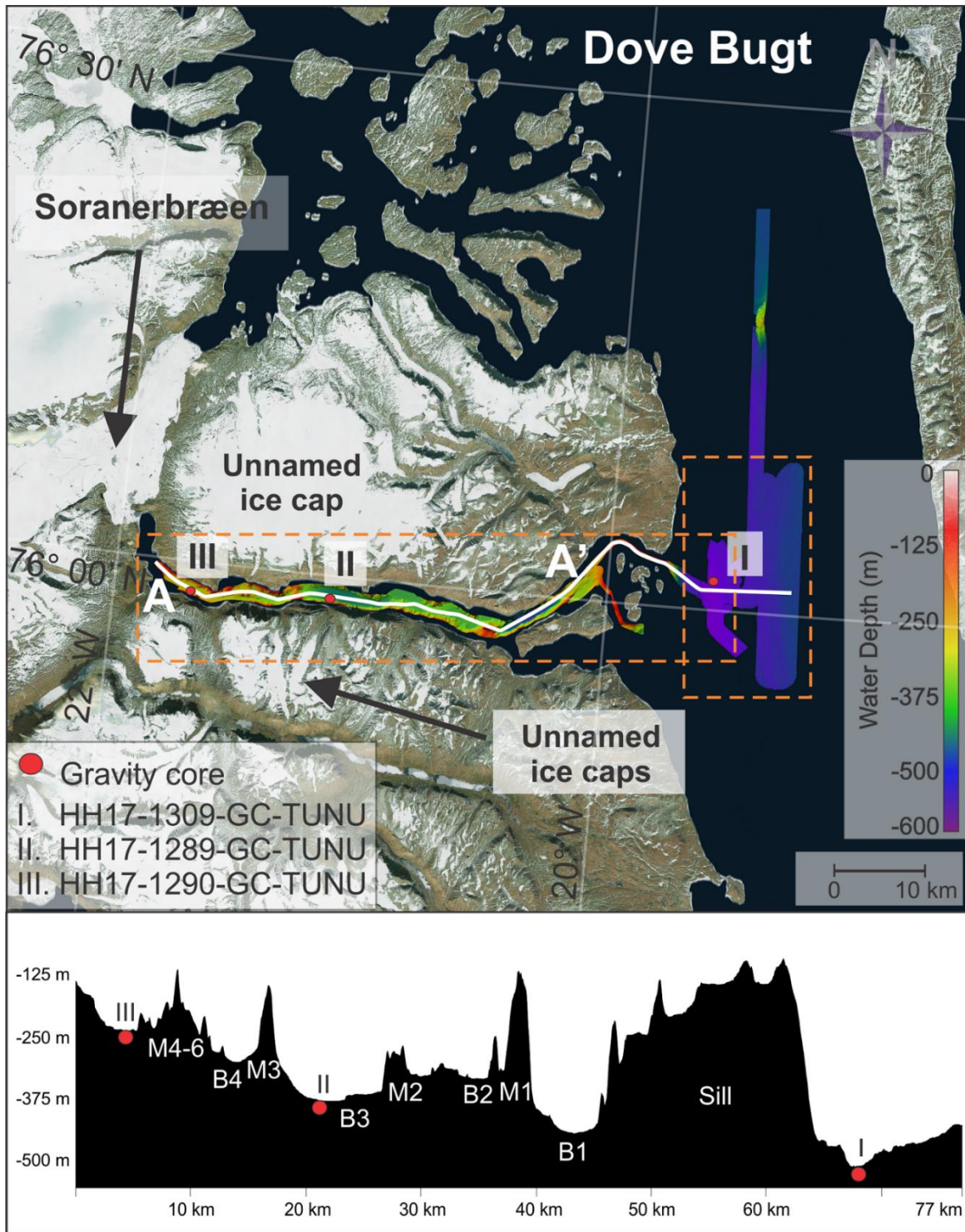
111 To the west of Bessel Fjord and Soranerbræen is the larger glacier L. Bistrup Bræ, which flows
112 northwards and has an outlet in Borgfjorden, another tributary fjord to inner Dove Bugt (Fig 1).
113 Here it is confluent with the southward flowing NEGIS outlet glacier, Storstrømmen (Rignot et
114 al., 2022). Studies of modern Soranerbræen, L. Bistrup Bræ and Storstrømmen suggest that
115 they all have separate drainage basins (Krieger et al., 2020). Storstrømmen and L. Bistrup Bræ
116 are two of the largest surge-type glaciers in the world (Higgins, 1991) with a surge periodicity of
117 approximately 70 years (Mouginot et al., 2018).

118 Bathymetry of inner Dove Bugt and tributary fjords has revealed that there are no natural large
119 passageways for the warm, salty, subsurface Atlantic Intermediate Water to impact these
120 glaciers at present, therefore it has been suggested that ocean waters do not play a large role in
121 the evolution of Storstrømmen, L. Bistrup Bræ and the northern outlet of Soranerbræen, and
122 that their grounding line retreat is mostly caused by ice thinning (Rignot et al., 2022).

123 Mega-scale glacial lineations (MSGSL) identified in Store Koldewey Trough on the continental
124 shelf have been interpreted as evidence for the expanse of this sector of the GrIS to the shelf
125 break during the LGM (Laberg et al., 2017; Olsen et al., 2020). This is further supported by the
126 presence of recessional moraines and grounding zone wedges, which suggests a complex
127 deglaciation of this part of the shelf area (Arndt et al., 2015, 2017; Laberg et al., 2017; Arndt,
128 2018; Olsen et al., 2020). Olsen et al. (2020) has suggested that deglaciation in the Store
129 Koldewey Trough may have occurred in two stages: first, an initial retreat as a result of eustatic
130 sea level rise caused by melting ice at lower latitudes (Lambeck et al., 2014), followed by a
131 melting phase driven by ocean warming. So far, the timing of the onset of the deglaciation is not
132 known. Across the GrIS, deglaciation is believed to be asynchronous, with factors such as
133 topography and local ice dynamics playing a large role with ice retreat in conjunction with
134 climate change (Bennike & Björck, 2002; Funder et al., 2011; Ó Cofaigh et al., 2013; Hogan et
135 al., 2016).

136 A recent study by Jackson et al. (2022) of the inner shelf east of the Clavering Ø (~74°N; Fig.
137 1b) indicated that during the late Younger Dryas, this sector of the GrIS had reached a more
138 landward position, in conformity with Funder et al. (2021). During this period the inner shelf
139 bottom water was characterized by anomalously high temperatures, interpreted to have played
140 a role in the ice retreat and leading to the termination of the Younger Dryas stadial. This was
141 followed by the onset of the East Greenland Current, as seen from cooler bottom water from the
142 Early Holocene on (Jackson et al., 2022).

143 Further north, east of marine terminating glacier Zachariae Isstrøm (~78° 30N; Fig. 1b), the
144 deglaciation of the NEGIS from the inner shelf was found to have occurred as early as 12.5 ka
145 cal BP, likely before 13.4 ka cal BP. Here, inflow of warmer water (Atlantic Water) may have
146 played a role. This part of the shelf was covered by an ice shelf from 13.4 to 11.2 ka cal BP
147 (including the Younger Dryas), retreating and leading to open water conditions from the earliest
148 Holocene; 11.2-10.8 ka cal BP, before readvancing from 10.8 to 9.6 ka cal BP, finally retreating
149 from 9.6 to 7.9 ka cal BP. At 7.9 ka cal BP there was a drastic shift in ocean circulation at this
150 site with a sharp decline in Atlantic Water corresponding to an increase in Polar Water influx
151 (Davies et al., 2022). Pados-Dibattista et al. (2022), studying another core from the NE
152 Greenland shelf (more seaward, in a mid-shelf position north of the Norske Trough at ~79°N),
153 found that during the early Holocene (9.4 to 8.2 ka cal BP), the East Greenland Current was
154 highly stratified with cold surface water overlying warm Atlantic subsurface water.



155

156 *Figure 2. Study area with the bathymetric data showing the locations of the sediment cores presented in this study.*
 157 *The lower panel is a profile along the length of Bessel Fjord, A-A'. Sediment cores are labelled I, II and III. Satellite*
 158 *image is displayed using a World Imagery satellite image (Earthstar Geographics, Esri, HERE, Garmin, FAO, NOAA,*
 159 *USGS) made available through GlobalMapper.*

160



161

162 *Figure 3. Image of an ice lobe from an ice cap near gravity core HH17-1289-GC-TUNU. Two sets of coarse-grained*
 163 *terminal morainal ridges are indicated by numbers and arrow. See Fig. 6b for the position of the modern ice lobe. The*
 164 *photograph was taken by Torger Grytå on a 2017 TUNU cruise.*

165 Following the 8.2 ka event, the interval from 8.2 to 6.2 ka cal BP was followed by the warmest
 166 Holocene bottom water conditions on the shelf. Afterwards, conditions returned to those seen
 167 prior to 8.2 ka cal BP due to increased Polar Water transport strengthening the East Greenland
 168 Current.

169 Terrestrial studies of Dronnings Margrethe II Land, Germania Land and adjacent areas have
 170 identified a complex assortment of moraines that are believed to have formed during the Kap
 171 Mackenzie, Muschelbjerg, Nanok I and Nanok II stadials (Hjort, 1979, 1981; Hjort and Björck,
 172 1983; Björck et al., 1994; Landvik, 1994). The exact ages of these stadials remain unclear
 173 (Table 1), yet Larsen et al. (2022) suggests that Nanok-stadial moraines found in Store
 174 Koldewey formed synchronously with the Milne Land moraines of Scoresby Sund which date to
 175 the Allerød to early Younger Dryas and Preboreal time (Kelly et al., 2008; Levy et al., 2016).

176 The position of striations on Store Koldewey and lateral moraines on coastal slopes between
 177 Bessel Fjord and Haystack have been interpreted as evidence for ice flowing out of Dove Bugt
 178 and Bessel Fjord during the Muschelbjerg stadal, southwards through Store Bælt and turning
 179 eastwards around the southernmost mountains of Store Koldewey (Hjort, 1981). Early studies of
 180 the region noted glacial and glaciofluvial deposits (e.g., moraine plateaux, terminal moraines,
 181 eskers and sandurs) on Hochstetter Forland that are believed to have formed during this period
 182 (Hjort, 1979, 1981).

183 Table 1. Previously published stadial information for the Dove Bugt region as well as age estimates used in this
 184 study.

Stadials	Studies					Age estimate used in this study
	<i>Hjort & Björck (1983)</i>	<i>Funder et al., (1998)</i>	<i>Kelly et al. (2008)</i>	<i>Vasskog et al. (2015)</i>	<i>Larsen et al. (2022)</i>	
<i>Nanok II</i>	10.1-9.5 ka cal BP	Preboreal (ending at ca. 9.7 ka cal BP)	Younger Dryas and Early Holocene (13-11.6 ka cal BP (G-III), 11.7-10.6 ka cal BP (G II))	Close to Bølling– Allerød transition, and late Younger Dryas (~14 ka cal BP (G III), ~12 ka cal BP (G-II))	Preboreal	Preboreal
<i>Nanok I</i>	Older than 14 ka cal BP, possibly between 15 and 19 ka cal BP				Late Allerød to early Younger Dryas	Late Allerød to early Younger Dryas
<i>Nanok 0</i>		~48 ka (Hjort, unpublished data)				?
<i>Muschelbjerg</i>	Saalian (or older)?					Saalian (or older)?
<i>Kap Mackenzie</i>	Saalian (or older)?					Saalian (or older)?

185
 186
 187 Lateral moraines and glacial striations oriented along the axis of Langsodal (also referred to as
 188 Langsødalen; Fig. 1c), a nearby valley south of and sub-parallel to Bessel Fjord, have been
 189 interpreted as evidence for glacial confinement within the valley during an undifferentiated
 190 Nanok stadial (Hjort 1979; Hjort, 1981). This differs from striations that have also been identified
 191 in the valley along more weathered surfaces that are oriented in a southwestern direction (Hjort,
 192 1979).

193 The outer coastal regions of North and Northeast Greenland are believed to have been
 194 deglaciated between 12.8 and 9.7 ka cal BP and present ice positions were reached between
 195 10.8 to 5.8 ka cal BP (Larsen et al., 2022). Cosmogenic nuclide dates from Store Koldewey, first
 196 collected by Håkansson et al. (2007), and later Skov et al. (2020) and Larsen et al. (2022),
 197 suggest that ice retreated from the continental shelf and reached the upper and lower sections
 198 of the island by 12.3 and 12.7 ka cal BP, respectively. In contrast, Biette et al. (2020) found
 199 evidence of the deglaciation of Clavering Ø at 16.2 ka cal BP, with readvances at 11.3, 10.8,
 200 3.3, 1.2 and 0.37 ka cal BP. Additional cosmogenic nuclide findings indicate that Trums Ø, in

201 outer Bessel Fjord, may have become deglaciated around 12.6 ka cal BP and Vandrepasset,
202 onshore inner Bessel Fjord, by 8.6 ka cal BP (Larsen et al., 2022).

203 Findings from macrofossil remains (Bennike & Björck, 2002) and lacustrine sedimentary records
204 (Cremer et al., 2008) suggest that coastal regions were deglaciated in a ~1500 year span after
205 the start of the Holocene (Klug et al., 2016). To the north of Store Koldewey, a minimum date
206 for deglaciation in Germania Land of 9.5 ka cal BP has been proposed (Landvik, 1994),
207 whereas to the south in southern Dronning Margrethe II Land, a minimum date of 11.2 ka cal BP
208 has been suggested (Bennike & Weidick, 2001). Lake studies on aquatic organisms at Björck
209 Lake and Hjort Lake on Store Koldewey (Fig. 1c) indicate that the island was at its warmest
210 between ~8 and 4 ka cal BP, (Wagner et al., 2008; Klug et al., 2009; Schmidt et al., 2011),
211 although findings from Melles Lake (Fig. 1c) suggest that the earliest onset of warmth during the
212 Holocene may have occurred at ~ 10 ka cal BP (Klug et al., 2009; Briner et al., 2016). On
213 Hochstetter Forland (Fig. 1c), pollen assemblages from Dødis Sø, Peters Bugt Sø and Ailsa Sø
214 suggest that the temperatures were at their highest between 8.8 and 5.6 ka cal BP (Björck &
215 Persson, 1981; Björck et al., 1994). These findings indicate that the HTM was not uniform
216 across East Greenland, as also described by Briner et al. (2016).

217 To the south, offshore the Kejser Franz Josef fjord system (~73°N), a detailed biomarker record
218 finds this part of the shelf dominated by seasonal sea ice throughout the late Holocene (<~5 ka
219 cal BP) and extended concentrations from 5.2 to 2.2 and 1.3 to present. Short-term variability
220 was also seen for this area for the last 2.2 ka cal BP, corresponding to the climatic events of this
221 period (Kolling et al., 2017).

222 **3. Material and Methods**

223 Swath bathymetry and three sediment cores were collected in southwestern Dove Bugt and
224 Bessel Fjord during an expedition aboard RV *Helmer Hanssen* of UiT The Arctic University of
225 Norway in September 2017, being part of the TUNU program (Fig. 2; Christiansen, 2012). The
226 swath bathymetry data was obtained using a Kongsberg Maritime Simrad EM 302 multibeam
227 echo sounder. It was gridded using Petrel software, and geomorphological interpretations were
228 made using Global Mapper 18. Surfaces were developed using a 5x5m grid cell size while a
229 surface created from an International Bathymetric Chart of the Arctic Ocean (IBCAO) dataset
230 4.0 with a 200x200m grid cell size (Jakobsson et al., 2020).

231 Two soft sediment gravity cores were retrieved from Bessel Fjord (HH17-1289-GC-TUNU &
232 HH17-1290-GC-TUNU) and one southwest of Dove Bugt in the sound Store Bælt (HH17-1309-
233 GC-TUNU) (Fig. 2 & Table 2). Prior to splitting the cores, physical properties were measured
234 using a GEOTEK Multi Sensor Core Logger (MSCL-S). The cores were placed in the laboratory
235 for 24 hours prior to obtaining physical measurements to ensure that each core temperature
236 reached equilibrium with the laboratory to avoid distorting p-wave values (Weber et al., 1997).

237 A GEOTEK MSCL X-ray Computed Tomographic imaging machine was also used to scan the
238 unopened core sections to create X-ray radiographic images. After each core was split and
239 cleaned, the characteristics of the sedimentary surface were logged (i.e., structures,
240 bioturbation, grain size, lithological boundaries, etc.), sediment color was noted using the
241 Munsell Soil Color Chart and lithofacies were assigned based on Eyles et al. (1983)
242 classification system. X-ray fluorescence (XRF) data (not published here), as well as colored
243 images of the core sections, were then obtained using an Avaatech XRF core scanner.

244 *Table 2. Information on the position, water depth and recovery length of each gravity core. Note that the core names*
 245 *are abbreviated in the text.*

Location	Inner Bessel Fjord	Mid-Bessel Fjord	Southeastern Dove Bugt
Coring station	HH17-1290	HH17-1289	HH17-1309
Latitude [N]	75° 58' 34.5907"	75° 58' 11.4928"	76° 01' 34.0387"
Longitude [W]	21° 07' 13.1055"	21° 41' 48.0278"	19° 34' 31.3190"
Water depth [m]	372	225	512
Recovery [cm]	534.5	245.5	474.55

246

247 Molluscs and benthic foraminifera were recovered from each core for the purpose of
 248 radiocarbon dating of lithofacies boundaries. This was, however, not always possible due to the
 249 low content of foraminifera and molluscs in these cores which also restricted the number of
 250 dates that could be obtained. Two adjacent 1 cm thick sediment slices were successfully
 251 sampled from select positions across cores HH17-1290 and HH17-1309. Samples were then
 252 wet sieved at 1 mm, 100 µm and 63 µm meshes, respectively. Benthic foraminifera from the
 253 100-µm size fraction were extracted for radiocarbon dating. Radiocarbon dating was carried out
 254 at the MICADAS radiocarbon laboratory at Alfred Wegener Institute, Helmholtz Centre for Polar
 255 and Marine Research, Germany. The radiocarbon dates were calibrated using the online
 256 version of OxCal 4.4 (<https://c14.arch.ox.ac.uk/oxcal.html#program>) and the Marine20
 257 calibration curve (Heaton et al., 2020), as the calibrated 14C samples are younger than 11.5 ka
 258 cal BP (Heaton et al., 2022). We are using a ΔR of -10 ± 60 in conformity with Jackson et al.
 259 (2022). Previously reported radiocarbon dates from this area that are relevant to our study have
 260 been recalibrated using Marine20 for marine samples under 11.5 ka and IntCal20 for terrestrial
 261 samples (Reimer et al., 2020). One marine sample older than 11.5 ka cal BP has also been
 262 included (Table 3). We are aware that for the Arctic, including our study area, calibration of
 263 marine samples by Marine20 is not recommended for samples older than 11.5 cal ka BP (see
 264 Heaton et al. (2022)), therefore, this calibrated age is treated with caution.

265 A Beckman Coulter LS 13 320 Multi-Wavelength Laser Diffraction Particle Size Analyzer was
 266 used to perform sediment grain size analysis. Sediment was sampled in mostly 10 cm intervals
 267 across HH17-1309, where samples taken from the other two cores were selected from specific
 268 positions. Samples were treated in HCl and H₂O₂ and a pre-heated VWB 18 Thermal Bath.
 269 Samples were then cleaned using distilled water, placed through multiple runs through a
 270 centrifuge and heated in an oven to remove water content. Approximately 0.2 grams of
 271 sediment were then separated and placed in a container with 20 ml of water and moved to a
 272 shaking table for over 48 hours. A few drops of Calgon were added to each sample, which was
 273 then placed into a Branson 200 ultrasonic cleaner for ~7 minutes and shaken briefly before
 274 being poured through a >2 mm mesh and into the particle size analyzer. Grains between the
 275 size of 0.4 µm and 2000 µm were counted and underwent three separate runs. GRADISTAT
 276 Excel-software was used to calculate the mean of the three runs. Sediment names used in
 277 reference to this analysis are based on Folk (1954) and mean grain size from the methodology
 278 published by Folk & Ward (1957).

279

280

281 Table 3. Other published radiocarbon dates and their recalibrated ages using Marine20 (and an ΔR of -10 ± 60 in
 282 conformity with Jackson et al. (2022)) and IntCal20 for aquatic moss samples. *The age of sample Lu-1298 from
 283 Shannon is above what is recommended by Heaton et al., (2022) for use with Marine20 and is therefore treated with
 284 caution.

Location	Material	Lab nr.	¹⁴ C age	¹⁴ C cal BP (1 σ range)	¹⁴ C cal BP (median)	Reference
Shannon	shell	Lu-1298*	19000 \pm 190	21855-22325	22078	Hjort, 1981; Hjort 1979
Hochstetter F.	shell	Lu-1289	9190 \pm 90	9572-9926	9779	Hjort, 1981; Hjort 1979
Shannon	shell	Lu-1389	9370 \pm 90	9865-10195	10015	Hjort, 1981; Hjort 1979
Hochstetter F.	shell	Lu-1386	9400 \pm 90	9896-10220	10054	Hjort, 1981; Hjort 1979
Hochstetter F.	shell	Lu-1300:1	9470 \pm 90	9970-10322	10157	Hjort, 1981; Hjort 1979
Hochstetter F.	shell	Lu-1300:2	9520 \pm 90	10084-10412	10229	Hjort, 1981; Hjort 1979
Hochstetter F.	shell	Lu-1384	9810 \pm 95	10409-10794	10617	Hjort, 1981; Hjort 1979
Ardencape Fjord	shell	Lu-1390	8570 \pm 85	8864-9200	9022	Hjort, 1981; Hjort 1979
Kildedalen	shell	Lu-1303	8930 \pm 90	9290-9573	9447	Hjort, 1981; Hjort 1979
Snenæs	Mya truncata, Hiatella arctica Nuculana	T-9372	8265 \pm 95	8434-8768	8619	Landvik 1994
Hvalrosodden moraine	pernula Nuculana	TUa-123	8685 \pm 95	9006-9315	9166	Landvik 1994
Hvalrosodden moraine	pernula	TUa-124	9045 \pm 90	9438-9741	9596	Landvik 1994
Hvalrosodden	Mya truncata	T-9361	8190 \pm 95	8360-8663	8523	Landvik 1994
Hvalrosodden	Mya truncata, Hiatella arctica	T-9370	7930 \pm 120	8681-9085	8890	Landvik 1994
Hvalrosodden	Mya truncata	T-9371	7490 \pm 115	8186-8502	8348	Landvik 1994
Peters Bugt	Portlandia	Ua-2787	10260 \pm 105	11071-11444	11253	Björck, 1994
Peters Bugt Sø	Hiatella arctica	Lu-3516	9640 \pm 90	10222-10527	10382	Björck, 1994
Storstrømmen Sound	Mya truncata & Hiatella arctica	K-6098	5180 \pm 95	5220-5520	5352	Weidick et al., 1994
Storstrømmen Sound	Mya truncata	K-5494	4910 \pm 85	4865-5175	5028	Weidick et al., 1994
Storstrømmen Sound	Mya truncata	K-5493	4840 \pm 90	4793-5117	4943	Weidick et al., 1994
Storstrømmen Sound	Hiatella arctica	Ua-3347	5030 \pm 75	5023-5311	5166	Weidick et al., 1994
Storstrømmen Sound	Hiatella arctica	Ua-3350	4180 \pm 60	3944-4225	4082	Weidick et al., 1994
Storstrømmen Sound	Balanoptera					
Storstrømmen Sound	physalus	K-6096	3630 \pm 90	3230-3530	3380	Weidick et al., 1994
Storstrømmen Sound	Hiatella arctica	Ua_3349	3725 \pm 60	3371-3616	3496	Weidick et al., 1994
Storstrømmen Sound	Hiatella arctica					
Storstrømmen Sound	& Mya truncata	K-6097	3230 \pm 85	2749-3024	2897	Weidick et al., 1994
Storstrømmen Sound	Hiatella arctica	Ua-3348	1815 \pm 55	1115-1317	1217	Weidick et al., 1994
Hjort Lake	Warnstorfia					
Hjort Lake	exannulata	Poz-6194	8260 \pm 50	8456-8722	8602	Wagner, 2008
Duck Lake	Aquatic moss	LuS-6525	8690 \pm 230	9527-10145	9775	Klug 2009

285

286

287

288

289

290 4. Results

291 4.1. Seafloor landforms in SW Dove Bugt (Store Bælt)

292 4.1.1. Elongated Lineations - Glacial Lineations

293 Slightly curved sub-parallel lineations, oriented sub-parallel to the axis of Dove Bugt, are the
294 most pronounced landforms in this part of the study area. They are oriented N-NW in the south
295 and N-NE in the north (Fig. 4). The most frequently identified positive lineations (ridges) are 35-
296 50 m in width, <1-3 m in height and between 1 and 10 km in length. Length to width ratios are
297 frequently >10:1. At elevations shallower than 435 m depth, near the center of Store Bælt, the
298 lineations are wider (e.g., 60-150 m wide), and occasional merging and overlapping of lineations
299 occur (Fig. 4e). Wider lineations, often identified in the southern section of the study area (Fig.
300 4b), have also been identified with widths, lengths and heights ranging from 200-650 m, 3-8 km
301 and 4.5-15 m, respectively. Length to width ratios here are 7:1 to >10:1. Some of the larger
302 lineations are superimposed by smaller lineations. Lateral ridges have also been identified in
303 clusters overprinting the lineations (Fig. 4c), where furrows have been found cross cutting
304 lineations (Fig. 4d). Lateral ridges measure 0.5 to 2 m in height and are approximately 45 to 250
305 m apart.

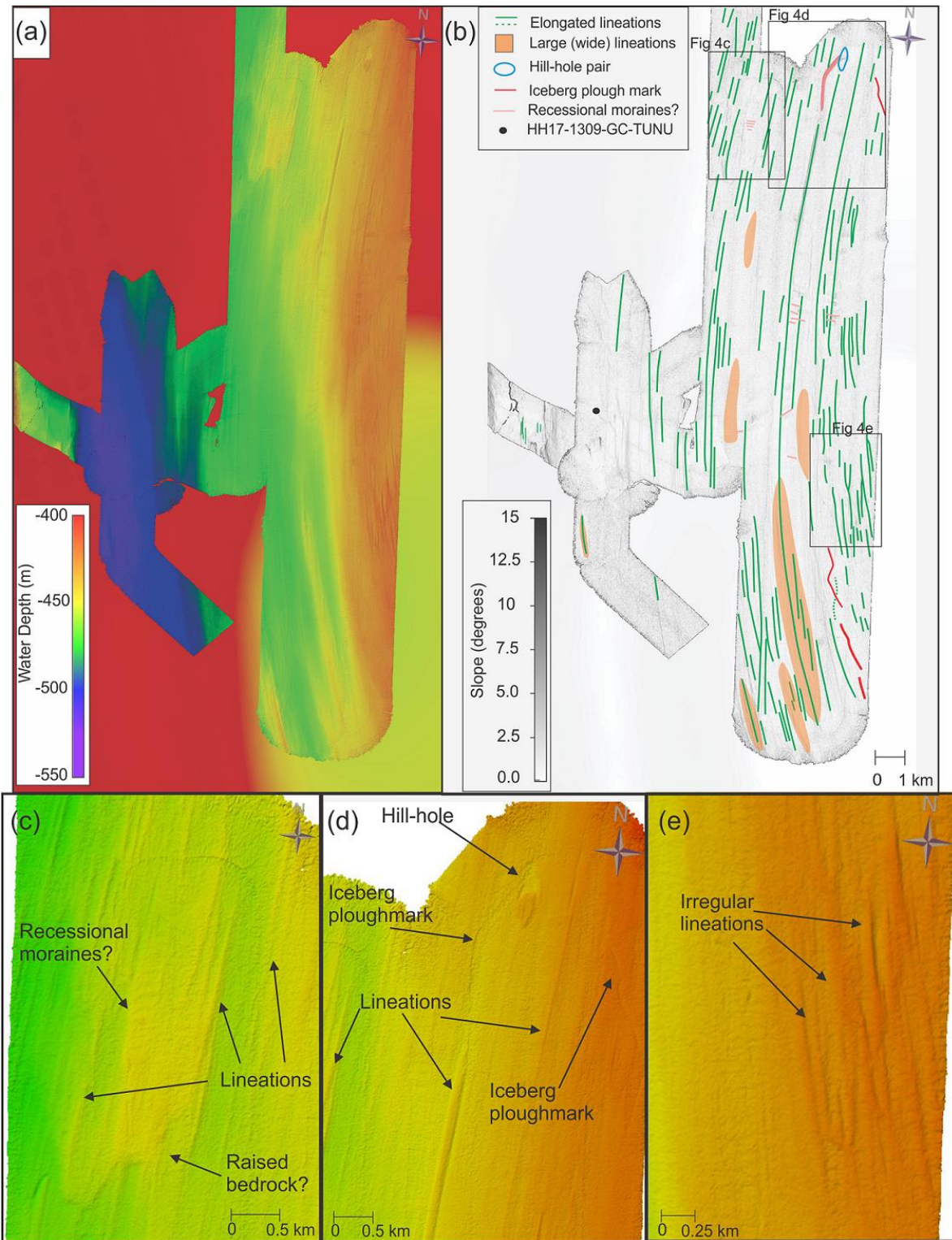
306 These elongated lineations are interpreted as glacial lineations (e.g., Ó Cofaigh, 2005). The
307 thinner, more common lineations (with length/width-ratios >10:1) have been interpreted as
308 mega-scale glacial lineations (MSGSL), and such landforms are commonly associated with
309 palaeo-ice stream environments (e.g., Stokes & Clark, 2001). Glacial lineations have been
310 identified in numerous continental shelf regions around Greenland (Evans et al., 2009;
311 Dowdeswell et al., 2014; Slabon et al., 2016; Laberg et al., 2017; Newton et al., 2017; Arndt,
312 2018; Batchelor et al., 2018; Jakobsson et al., 2018). While the mechanism behind the
313 formation of these features are still being debated, some authors have suggested that they may
314 have formed through meltwater flooding (Shaw et al., 2008), groove-ploughing (Clark et al.,
315 2003) or the transverse flow in basal ice (Schoof and Clarke, 2008). King et al. (2009), who
316 viewed the formation of MSGSL in real time in West Antarctica favored aspects of the dilatant till
317 instability model, but with till properties that could explain ribbed moraine formation and the
318 development of these landforms on a decadal timescale. Sets of ridges that overprint the glacial
319 lineations have been interpreted as recessional moraines, where furrows have been interpreted
320 as iceberg plough marks.

321 4.1.2. Depression and Mound- Hill-Hole Pair

322 In northern Store Bælt, a 200 by 450 m wide, 3-4 m deep depression has been identified next to
323 a mound with a width and height of 235 by 450 m and 3-4 m, respectively (Fig. 4d). The
324 depression overprints N-S trending lineations, although the mound contains lineations on its
325 surface.

326 This depression and mound have been interpreted as a hill-hole pair. These landforms can form
327 when ice-thrust rafts of sediment are removed from the bed by cold-based, slow-flowing ice that
328 transports the sediment that was once in the depression (Hogan et al., 2010; Klages et al.,
329 2013, 2015). In this instance, a south bound ice stream may have removed frozen sedimentary
330 material and deposited it further south.

331



332

333 *Figure 4. Bathymetric maps from SW Dove Bugt. (a) Seafloor relative to water depth with IBCAO 4.0 displayed in the*
 334 *background (Jakobsson et al., 2020). (b) The main landforms and slope angles of the seafloor in SW Dove Bugt.*
 335 *Locations of Figs. 4c-e are indicated. (c) Bathymetry of the northwestern section of the study area. (d) Bathymetry of*
 336 *the northeastern part of the study area. (e) Bathymetry of the eastern part of the study area showing irregularly shaped*
 337 *glacial lineations.*

338 4.2. Sea floor landforms in Bessel Fjord

339 4.2.1. Large scale geomorphology

340 Bessel Fjord contains a variety of basins that are separated by different styles of sills (Figs. 2, 5
341 & 6). The outermost sill is at the fjord's entrance, and it commonly ranges in depth from 50 to
342 200 m, with major sections reaching above (and near) the water surface as there are islands in
343 the fjord entrance. Four large basins that are elongated in a west-east direction have been
344 identified in Bessel Fjord (B1-B4). The deepest basin, Basin 1 (B1), is the closest to the fjord
345 entrance and is separated from basin 2 (B2) by a >215 m high sill (M1) that is steeper to the
346 east (Figs. 2 & 5). Basin 3 progressively deepens westwards, with a maximum depth of 380 m.
347 A ~70 to 160 m asymmetrical sill (M3; Figs. 2 & 5) that is steeper on its east side separates
348 Basin 3 from basin 4. Basin 4 is the shallowest basin (~280-300 m) and is adjacent to multiple
349 smaller basins that are primarily at lower points of elevation. The fjord also contains smaller
350 basins that are raised relative to the average seafloor depth (Fig. 6e). Features interpreted as
351 bedrock mounds have also been identified in other sections of the fjord (Figs. 5 & 6). Along the
352 fjord sides, landforms from sediment reworking including slide scars, channels and gullies have
353 also been observed Fig 6b.

354 4.2.2. Linear Ridges Oriented Along Fjord Axis- Glacial Lineations

355 Oriented along the fjord's axis (or at times slightly oblique to it), linear features have been
356 identified in the inner and middle of the fjord, as well as a single lineation on the outer part of the
357 fjord (Figs. 5 & 6). They range in size from 100 to 1000 m in length and ~3 to 9 m in height,
358 although some that are as high as 80 m have been identified in the inner fjord. Their
359 morphologies vary throughout the fjord, and their length to width ratios range from 2:1 to 5:1.
360 Most ridges slope towards the outer fjord, although some slope in the opposite direction or have
361 an irregular or flat top. They appear both independently in connection with inferred bedrock
362 highs, and in clusters in flat lying areas of basin 3. These ridges have been interpreted as
363 glacial lineations, and they are thus indicating the direction of former glacier flow.

364 4.2.3. Transverse Ridges- Moraines

365 Several transverse ridges have been identified in the inner and central portion of the fjord,
366 oriented perpendicular to the fjord's axis (Figs. 2, 5 & 6). The ridges in the inner most position of
367 the fjord tend to largely conform to the topography (i.e., between bedrock mounds, some of
368 which are position mid-fjord (M4-6; Fig. 6b), and the fjord sidewalls) and are the threshold
369 between sub-basins (Fig. 6). The width and length of ridges range from 150 to 600 m and 120 to
370 500 m, respectively, where their heights are between <5 to 58 m.

371 A particularly large, asymmetrical transverse ridge that spans the width of the fjord, is situated
372 between Basin 3 and 4 (M3; Figs. 2 & 6d). This ridge is ~1.5 km in width and between 72 to 162
373 m in height. It contains a crescent shape in aerial view and is concave towards the mouth of the
374 fjord. A large threshold with a 1.8 km width and a > 215 m height also separates basin 1 and 2
375 (M1; Figs. 2 & 5). This feature is ~150m shallower in the north and dips steeply into basin 1.

376 The transverse ridges have been interpreted as moraines, which would have formed during
377 glacial stillstands or readvancements during the retreat of a grounded tidewater glaciers margin.
378 These moraines do not fill the width of the innermost fjord, which has also been seen in inner
379 Nordfjord (part of the Keiser Franz Josef fjord system) by Olsen et al. (2022). While the large
380 transverse ridge M3 is believed to be a moraine, it is considered more likely that M1 is a
381 bedrock mound based on its morphology. The smaller transverse ridges are interpreted as
382 recessional moraines. Smaller moraines have the potential to form at ice margins annually

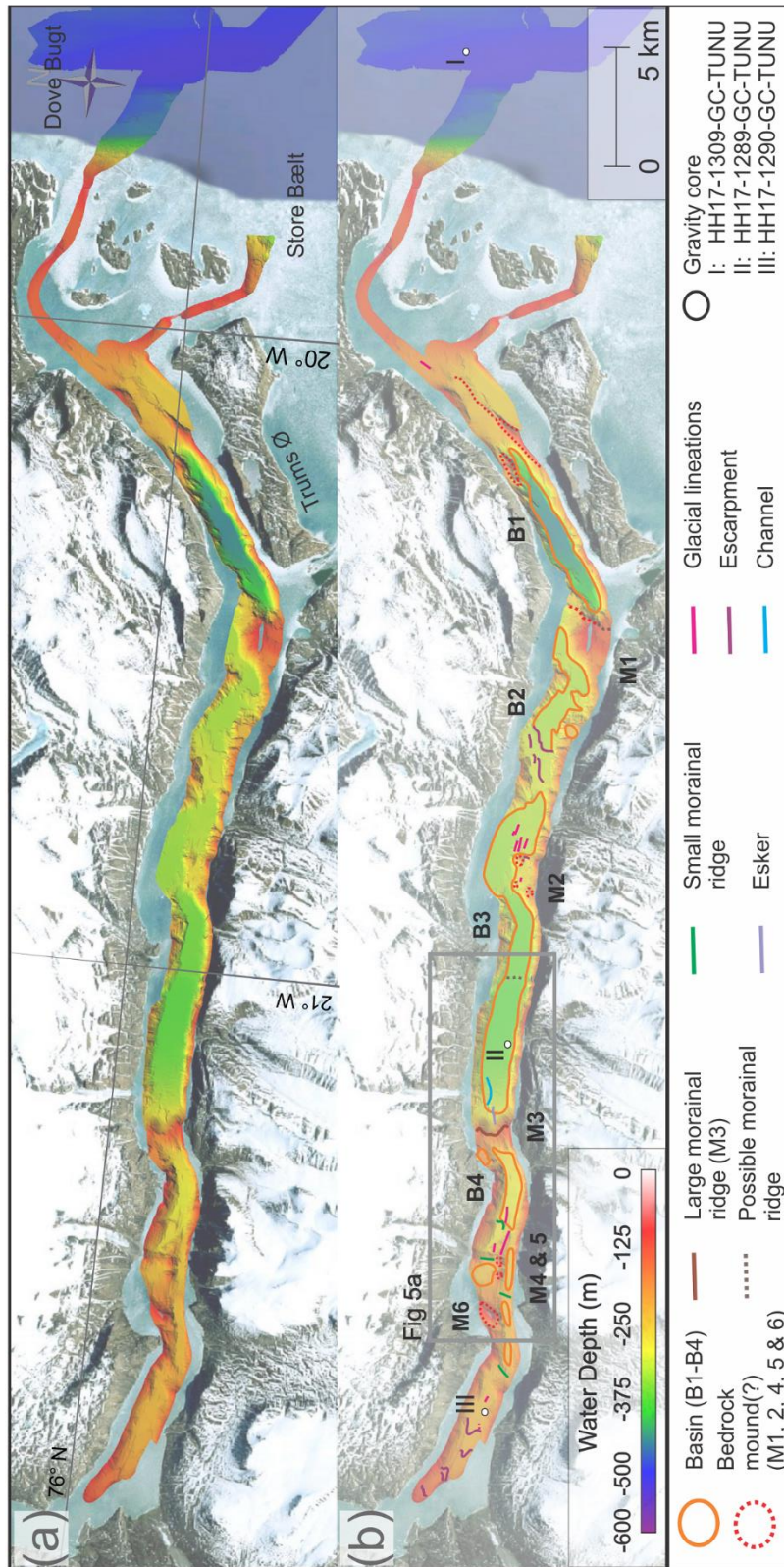
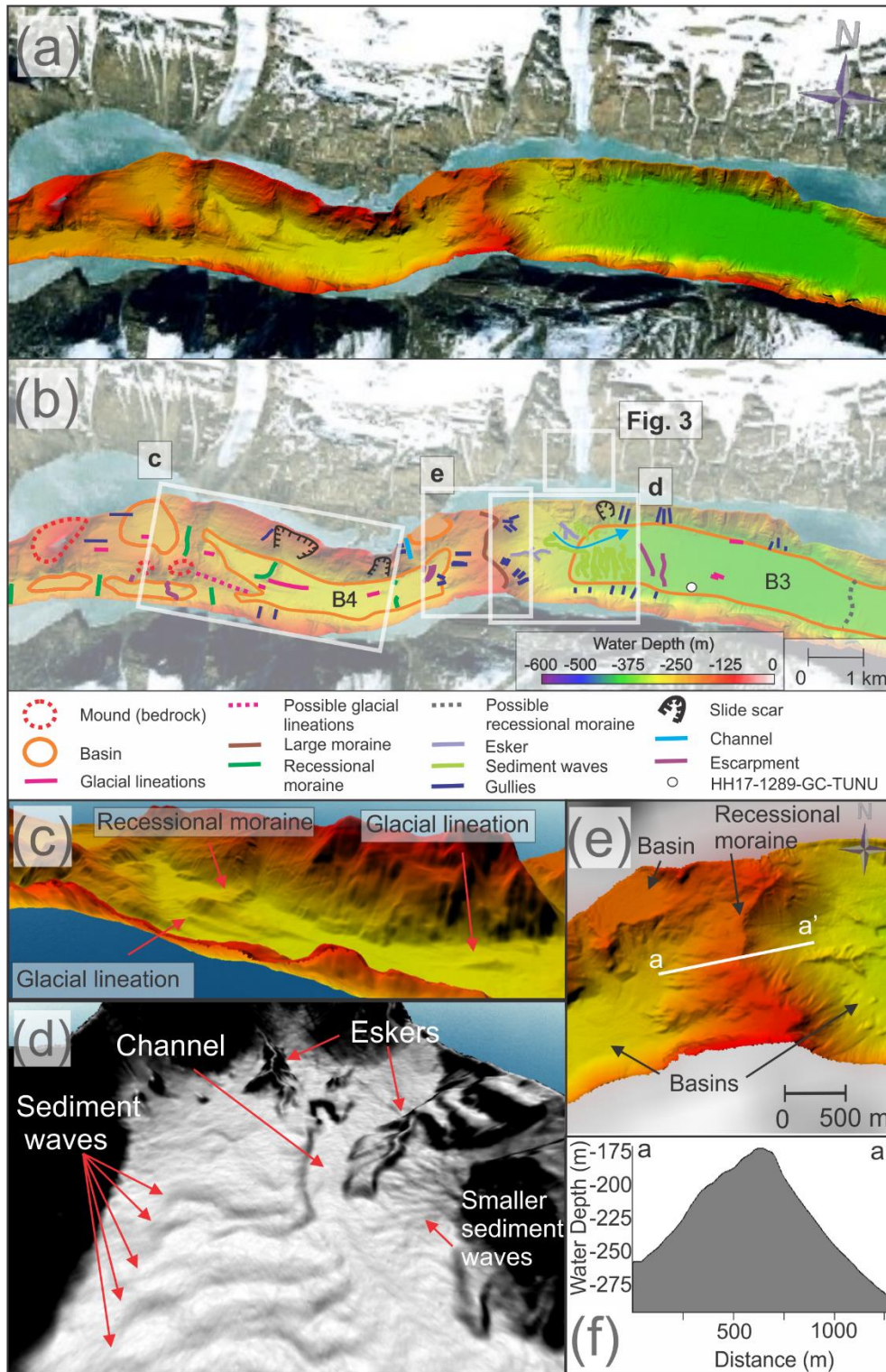


Figure 5. (a) Bathymetric map of Bessel Fjord. (b) A map of mapped features in Bessel Fjord. Satellite images obtained from Google Earth (© Google 2020).



386

387 *Figure 6. (a-b) Mapped sections from inner to middle Bessel Fjord. Background images used for 6a & 6b obtained*
 388 *from Google Earth (© Google 2020). (c) Glacial lineations in Basin 4 (B4). (d) Eskers, sediment waves and a channel*
 389 *in Basin 3 (B3). (e) A large moraine (M3) between B3 and B4. Note the raised sub-basin to the west and esker to the*
 390 *east. (f) Profile across the large recession moraine (M3).*

391 (Lyså & Vorren, 1997; Dowdeswell et al., 2016) and have been observed with a variety of sizes
392 and morphologies on the NE Greenland shelf (e.g., Winkelmann et al., 2010).

393 *4.2.4. Sinuous Ridges- Eskers*

394 Sinuous ridges, oriented parallel or oblique to the fjord's axis, occur in basin 3 (Figs. 5, 6b, 6d
395 &6e). These features have widths and lengths of 50 to 120 m, 350 to 800 m, respectively and
396 heights of 10 to 15 m. The most pronounced examples of these ridges have been observed east
397 of the large recessional moraine that has been previously discussed (Fig. 6e).

398 These sinuous ridges have been interpreted as eskers. These landforms form from sediment
399 infill of subglacial and englacial conduits and have been identified in other studies in Greenland
400 (Huddart and Lister, 1981; Geirsdóttir et al., 2000; Winkelmann et al., 2010; Lane et al., 2015).
401 They frequently form in the direction of former ice flow and often form during terminal stages of
402 glaciation, and are therefore associated with moraines (Shreve, 1985). They vary in size
403 depending on the glacial drainage pattern, as well as a number of other factors, however eskers
404 identified within Bessel Fjord appear smaller than those identified in studies in Canada, the UK
405 and Kola Peninsula in Russia (Storrar et al., 2014).

406 *4.2.5. Wavy Transverse Ridges- Sediment Waves*

407 Adjacent to the two eskers in Basin 3 are a series of wavy transverse ridges to the east of a
408 large recessional moraine (Figs. 5, 6b & 6d). These features occupy an area of ~500 by 1500 m
409 and contain small ridges and flat areas that slope at an angle of 3 to 6° to the east. Each wave
410 "crest" is ~50 to 100 m apart, although some appear to begin only halfway through the width of
411 the area, where others occupy the entire width, north to south. These waves are crosscut by a
412 channel to the north (Fig. 6d). North of this channel similar features with a wavy morphology
413 occur, although these are substantially smaller.

414 These wavy transverse ridges have been interpreted as sediment waves. Sediment waves
415 found associated with deltaic and glacialfluvial deltaic systems have been associated with
416 retrogressive slope failures, gravity-induced sediment creep and/or the migration of sediment
417 waves upslope (Cartigny et al., 2011; Hill, 2012; Stacey and Hill, 2016). Alternatively, given the
418 position of the smaller wavy transverse ridges to the ice cap on Ad. S. Jensen Land (Figs. 1 &
419 2) and the larger ridges to the large moraine to the west (Figs. 5 & 6) it is also possible that
420 these ridges are sets of moraines. Recessional moraines have been identified in the vicinity of
421 eskers in Spitsbergen fjords (Ottesen et al., 2008; Kempf et al., 2013), which may account for
422 the smaller wavy transverse ridges. The larger wavy transverse ridge do also resemble thrust
423 moraines identified by Forwick et al. (2010). Further work may be required in the evaluation of
424 these features. For a full list of observed landforms see Table 4.

425 *4.3. Lithostratigraphy*

426 Three gravity cores were retrieved from the study area. Gravity core HH17-1309 was collected
427 in Store Bælt and was sampled from a N/NW-S/SE oriented depression that contains iceberg
428 ploughmarks and a MSGL. Gravity core HH17-1289 was collected in the middle of the Bessel
429 Fjord and is located directly east of the above-mentioned sediment waves on the distal part of
430 the pronounced transverse ridge. Nearby, a modern ice cap fed glacialfluvial channel is observed
431 in satellite imagery, likely with a delta at its fjord termination. The gravity core HH17-1290 was
432 collected within the inner fjord, west of the basins and thresholds observed in this study area
433 and is the closest core to Soranerbræen (located ~9.7 km east of the glacier) (Fig. 7).

434

435 Table 4. Overview of observed landforms in southern Dove Bugt and Bessel Fjord.

Region	Description	Width	Length	Height	Notable Feature	Interpretation
Dove Bugt	Elongated lineations	35-50 m	~1->10 km	<1-3 m	Roughly N-S	Glacial Lineations
	*Wide	200-650 m	3.8 to 8.8. km	4.5-15 m		
	Depression and mound	200 m	450 m	3-4 m	Mound to the south of the depression	Hill-hole pair
	Furrows (scour marks)	~40-100 m	<100-200	3-5 m	Irregular	Iceberg plough marks
	Transverse ridges	150-400 m	~30-100 m	0.5-1 m	Roughly W-E	Recessional moraines
Bessel Fjord	Linear ridge	45-350 m	100-1000 m	3-9, 80 m	Parallel to the fjords axis	Glacial Lineations
	Transverse ridges	150-600 m	120- 500 m	<5-58 m	Perpendicular to the fjords axis	Recessional moraines
	*Large ridge (M3)	1485 m	600-1600 m	72 to 162 m		Moraine
	Sinuuous ridges	50-120 m	350-800 m	10-15 m		Esker
	Wavy transverse ridges	400-700 m	~45-100 m	2-5 m	Perpendicular to the fjords axis	Sediment wave
	Elongated depression	~200 m	~1 km	6-8 m		Channels
	Chute	~20-100 m	60-400 m	1-15 m		Gullies

436

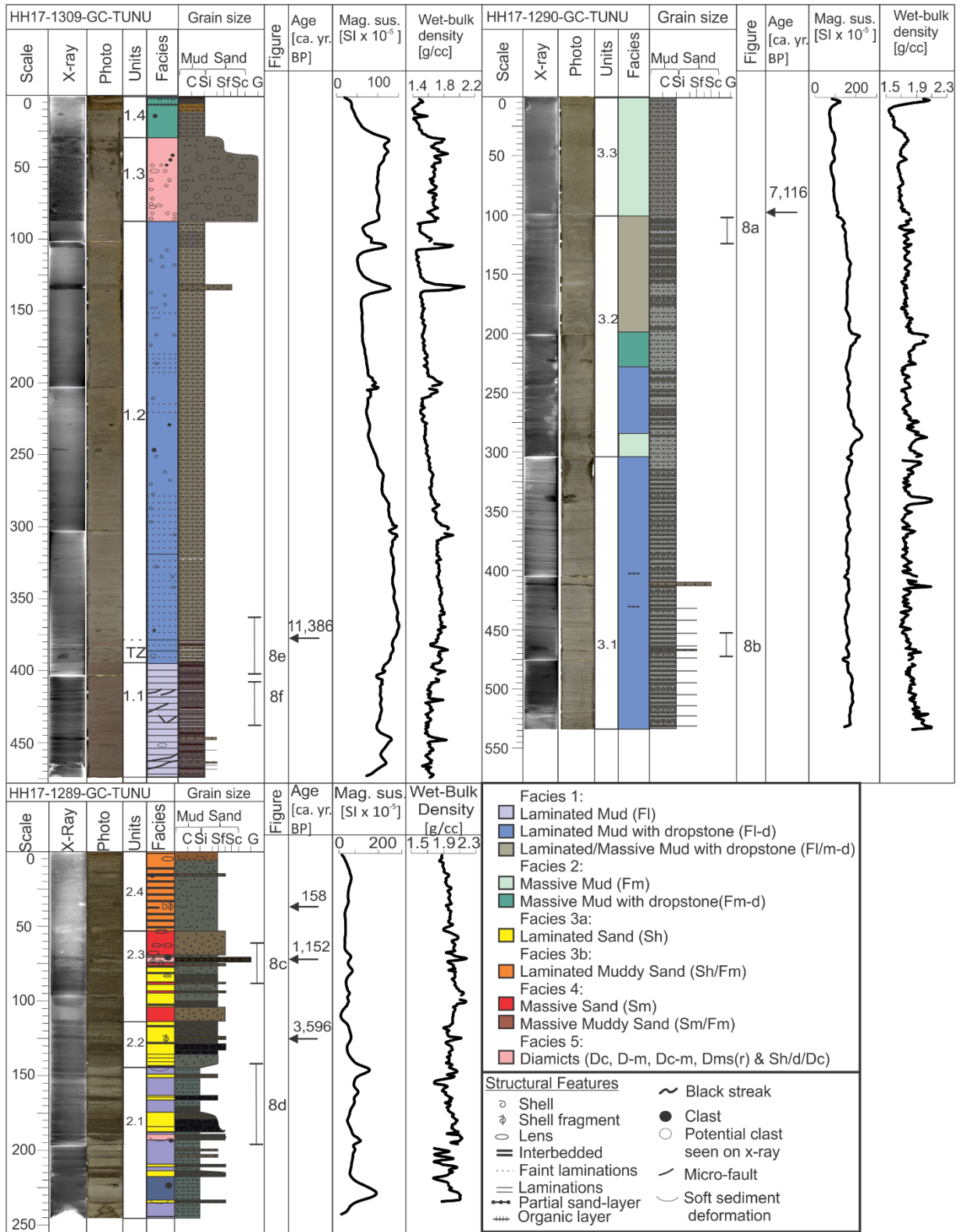
437 **4.3.1. Facies**

438 *Facies 1 – Laminated Mud (FI, FI-d & FI/m-d)*

439 Facies 1 consists of laminated mud (FI) and laminated mud with dropstones (FI-d) and have
 440 been observed in all three gravity cores (Figs. 7, 8a, 8d & 8f)). Laminations are composed of
 441 either mud or very fine sand. Mud laminations with finer laminations have also been identified in
 442 Unit 3.2 (100-200 cm; Fig. 7a, FI/m-d). Microfractures have also been identified within this facies
 443 (Fig. 8f).

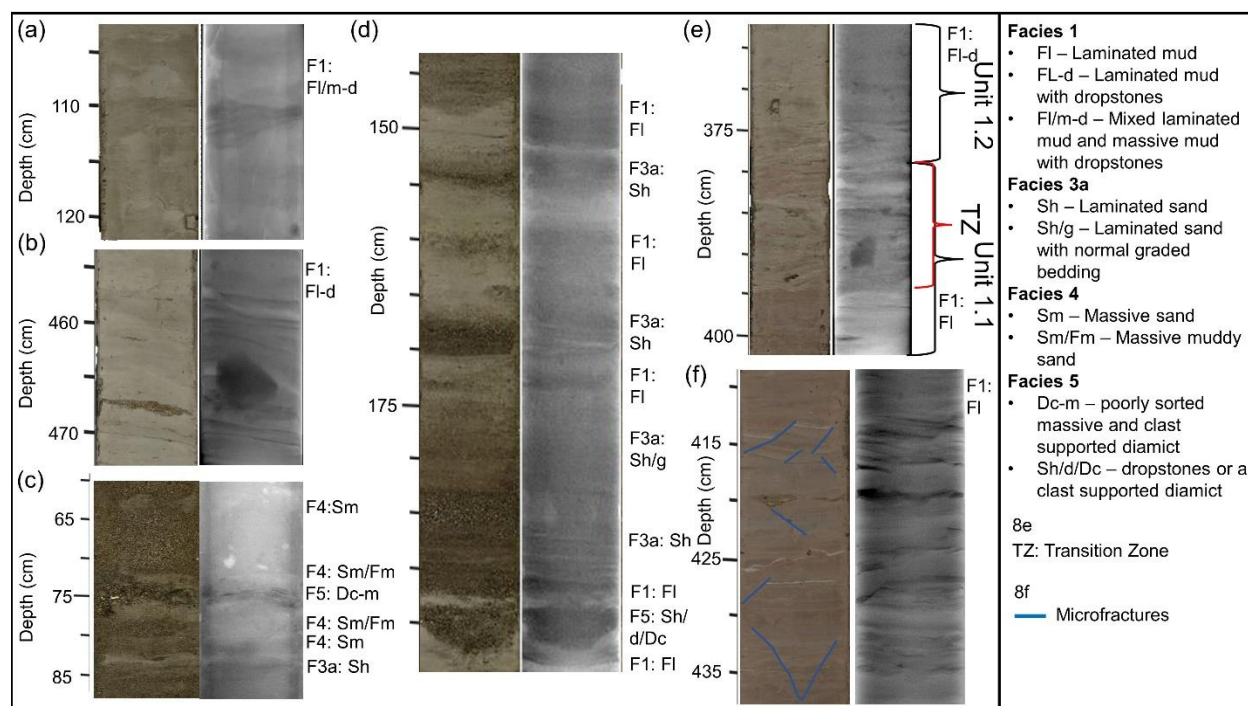
444 Wet-bulk density measurements tend to increase with depth in some sections of this facies
 445 (e.g., 87-350 cm in HH17-1309), suggesting normal sediment consolidation. However, a
 446 stagnation or decrease in wet-bulk density with depth in other sections (e.g., below ~350 cm in
 447 HH17-1309) suggests less consolidation. The magnetic susceptibility generally tends to
 448 increase with depth in HH17-1309 and in Unit 3.2 in HH17-1290, however the remainder of this
 449 facies in HH17-1290 (Unit 3.1) remains relatively stable to the base of the core. Notable positive
 450 peaks have been identified at 110 and 140 cm in HH17-1309 and measurement fluctuations
 451 occur in HH17-1289. Peaks in magnetic susceptibility may reflect the introduction of turbidites or
 452 clasts where fluctuations may reflect shifts in sediment provenance.

453 Muds with sand laminations are believed to have formed through a combination of ice-proximal
 454 suspension settling from overflow plumes and turbidity-current activity (underflows). The
 455 rhythmically laminated muds are believed to have formed from ice-proximal suspension settling
 456 from turbid overflow plumes. Similar laminated sediments have been identified in Kejsler Franz
 457 Joseph Fjord and Fosters Bugt in East Greenland and are theorized to have been deposited



458

459 Figure 7. Lithological core logs of the three gravity cores with x-ray images, core photos, unit divisions, facies,
 460 structures, magnetic susceptibility and wet-bulk density. TZ in HH17-1309-GC-TUNU stands for "Transition Zone".
 461 Grain size abbreviations: C: clay, Si: silt, Sf: fine grained sand, Sc: coarse grained sand and G: gravel.



463

464 *Figure 8. Photographic and x-ray images of sections of the three gravity cores (a-f). Corresponding facies codes can*
 465 *be found to the right of each image.*

466 from turbid meltwater plumes in an ice-proximal environment (Evans et al., 2002). Large clasts
 467 have been interpreted as ice rafted debris (IRD). The formation of microfractures may have
 468 been caused by soft sediment deformation, possibly from grounded icebergs.

469 *Facies 2 – Massive Mud (Fm & Fm-d)*

470 The second facies consists of massive mud with or without dropstones and can be found in the
 471 inner fjord core HH17-1290 and the Store Baelt core HH17-1309 (Fig. 7). In HH17-1290 this
 472 appears downcore between sections of Facies 1 as well as in the topmost unit, Unit 3.3. The
 473 magnetic susceptibility gradually increases downcore in this facies in Unit 3.3. Further down
 474 core, in Unit 3.2, this facies is associated with a downwards trend in magnetic susceptibility
 475 following peaks in measured readings. Wet bulk density values roughly mirror these trends. In
 476 HH17-1309 massive mud units have been observed in Unit 1.4, where magnetic susceptibility
 477 and wet bulk density values increase downcore.

478 This facies is interpreted as being the result of suspension settling from overflow plumes and is
 479 believed to have been deposited in an ice-distal glacial marine environment with varying input from
 480 IRD (i.e., Boulton & Deynoux, 1981). Sediment may be sourced from a single location (i.e.,
 481 Soranerbræen) or more than one location (e.g., local ice caps) in an ice-distal glacial marine
 482 environment with limited iceberg or sea-ice rafting. Massive mud deposits have also been
 483 identified in other Greenland fjords (e.g., Ó Cofaigh et al., 2001) and it has been suggested that
 484 they may indicate meltwater from ice- or fjord margin-distal conditions (Evans et al., 2002).

485 *Facies 3a – Laminated Sand (Sh)*

486 Facies 3a consists of sections of sand with horizontal sand laminations. This facies has been
487 predominantly observed in the mid-fjord core, HH17-1289-GC-TUNU (Figs. 7 & 8d). These
488 sections consist of fine to medium grained sand that range in thickness and colors. Occasionally
489 this facies also contains normal graded bedding (e.g., Fig. 8d, ~174-183 cm). This facies does
490 not contain uniform magnetic susceptibility or wet-bulk density readings as it has been found in
491 association with low and high peaks of both parameters as well as values that are near the
492 average for the core.

493 This facies is interpreted as being deposited from turbidity currents, possibly underflows that are
494 either sourced from glacial or non-glacial streams and slope failures. Uniform layers may
495 indicate a single, rapid event, where shifts in grain size and color may be the result of short-lived
496 fluctuations in sediment input. Laminated sands have been identified in Scoresby Sund in East
497 Greenland and have also been attributed to turbidite formation (Ó Cofaigh et al., 2001).

498 *Facies 3b – Laminated Muddy Sand (Sh/Fm)*

499 Facies 3b represents sections of sand with faint horizontal laminations as well as a large
500 quantity of clay material interspersed throughout with faint laminations. This has been observed
501 in HH17-1289 at the topmost unit in the core, Unit 2.4 (Fig. 7). Magnetic susceptibility is
502 relatively uniform in this facies, where the wet-bulk density tends to decrease up core. Sediment
503 grain size analysis of a single sample from this facies revealed that the sediment is composed
504 of 56.3% sand and 43.7% mud. A “patch” of black organic material (i.e., plant material and
505 shells) was also identified within this unit.

506 This complex facies is believed to have formed predominantly from underflow events, sandy –
507 muddy turbidites, alternatively sandy turbidites with additional input from suspension settling.
508 Similar deposits have been observed in Balsfjord, Norway although without lamination and
509 possibly a higher mud content (Forwick and Vorren, 1998).

510 *Facies 4 – Massive Sand / Massive Muddy Sand (Sm & Sm/Fm)*

511 Facies 4 contains sections of massive sand (Sm) as well as massive sand with a large amount
512 of clay content (Sm/Fm). This facies is predominantly found in Unit 2.3 (and to a much less
513 extent, Unit 2.4) in HH17-1289 (Fig. 7). Sections of massive sand have been found in
514 association with mud lenses and often contain horizontal sand layers (Sh) above and below it.
515 Slight increases and decreases in magnetic susceptibility values have been observed within this
516 facies.

517 This facies is believed to have developed through rapid deposition as well as deformation of
518 Facies 3a & b. According to this interpretation, the mud lenses observed in this facies were
519 once layers/lamina that became deformed due to the sand – mud density contrast. Massive
520 sand has been found in Kangerlussuaq and Miki Fjords in East Greenland (Smith and Andrews,
521 2000) and well-sorted coarse grain deposits have been recovered near Petermann Glacier in
522 northern Greenland (Reilly et al., 2019). Authors have attributed these layers to sediment gravity
523 flows.

524 *Facies 5 – Diamicts (Dc, D-m, Dc-m, Dms(r) & Sh/d/Dc)*

525 Facies 6 contains a variety of different diamicts observed within the mid-fjord core HH17-1289
526 and the Store Baelt core HH17-1309. In HH17-1289 this includes a 3.5 cm poorly sorted
527 massive and clast supported diamict (Dc-m) in the middle of Unit 2.3 (Figs. 7 & 8c), and a
528 horizontally laminated layer of sand that that is either accompanied by dropstones or a clast

529 supported diamict (Sh/d/Dc) (Figs. 7 & 8d). It is inferred that they are the result of sea ice or
 530 iceberg rafting/dumping. Within HH17-1309 there is a substantially larger, sharp based, matrix-
 531 supported diamict, stratified in its upper part (Dms(r)) in Unit 1.3 (Fig. 7). Based on these
 532 characteristics, this diamict has been interpreted as a density flow deposit, likely a debris flow
 533 deposit that is overlain by (part of) a turbidite.

534 4.3.2. Chronology and sedimentation rates

535 Shell and shell fragments were recovered from HH17-1289 for radiocarbon dating. At 34 cm
 536 depth, a semi-spherical path of organic content was identified, containing two intact *Yoldiella*
 537 *lenticula*, a shell fragment and plant material. Additionally, at 71 cm depth, a large 3 cm half of a
 538 *Hiatella arctica* shell was collected for dating, and shell fragments were recovered from a depth
 539 of 125 cm for the same purpose. These shells yielded radiocarbon ages of 158, 1,152 and
 540 3,596 cal yr. BP, respectively (Table 5).

541 Cores HH17-1290 and HH17-1309 were subsampled for foraminifera material at four positions.
 542 Calcareous benthic species, which were rare, were used for dating and include predominantly
 543 *Melonis barleeanus* as well as *Islandiella norcrossi*, but in substantially smaller quantities. In
 544 HH17-1309, at a depth of 377 cm *Islandiella norcrossi* (rare to common) & *Stainforthia feylingi*
 545 (rare) and a planktonic species were identified immediately above the transition zone between
 546 deformed (below) and undeformed sediments (above). Radiocarbon dates for the HH17-1309
 547 sample yielded an age of 11,386 cal yr. BP where the sample from HH17-1290 yielded an age
 548 of 7,116 cal yr. BP (Table 5).

549 Table 5. Radiocarbon dates, calibrated dates, and associated linear sedimentation rates.

Coring station	Sampling Depth [cm]	Lab nr.	Species	¹⁴ C age BP	Marine20 cal BP (1σ range)	Marine20 cal BP	Linear sedimentation interval [cm]	Linear sedimentation rate Marine20 [cm/ka]
HH17-1309-GC-TUNU	377	5157.1.1	Mixed benthic foraminifera	10357 ± 95	11201 - 11553	11386	0-377	33.11
HH17-1289-GC-TUNU	35	5154.1.1	<i>Yoldiella lenticula</i>	688 ± 34	61 - 253	158	0-35	221.52
HH17-1289-GC-TUNU	71	5155.1.1	<i>Hiatella arctica</i>	1747 ± 28	1065 - 1250	1152	35-71	31.25
HH17-1289-GC-TUNU	125.5	5156.1.1	Bivalve frag.	3809 ± 36	3472 - 3701	3596	71-125.5	15.16
HH17-1290-GC-TUNU	97	5158.1.1	Mixed benthic foraminifera	6800 ± 80	6990-7250	7116	0-97	13.63

550
 551 Linear sedimentation rates were calculated assuming modern sediments are at the core top as
 552 no overpenetration was recorded during the sampling of these cores and that during the core
 553 logging little sediment disturbance was found (Table 5). Given the scarcity of biological material
 554 in these cores these sedimentation rates act only as a first approximation until a more detailed
 555 record can be recovered. Using the available (calibrated) dating results, sedimentation rates of
 556 ~15 cm/ka, ~31 cm/ka, & ~222 cm/ka were calculated for core HH17-1289 at 71-125.5 cm, 35-
 557 71 cm, and 0-35 cm, respectively. These results reveal an increase in the sedimentation rate
 558 towards the present. However, as this core includes multiple deposits from turbidity currents

559 (i.e., reworked deposits), linear sedimentation rates in core HH17-1289 should be treated with
560 caution. An average, linear rate of ~14 cm/ka was calculated for the interval of 0-97 cm in core
561 HH17-1290 and an average, linear rate of ~33 cm/ka was also obtained for the large interval of
562 0-377 cm in core HH17-1309. These linear rates are lower, up to an order of magnitude, when
563 compared to the Kejser Franz Josef Fjord system ~400 km south of the study area (Olsen et al.,
564 2022). The origin of this observed difference must await further studies.

565 **5. Discussion**

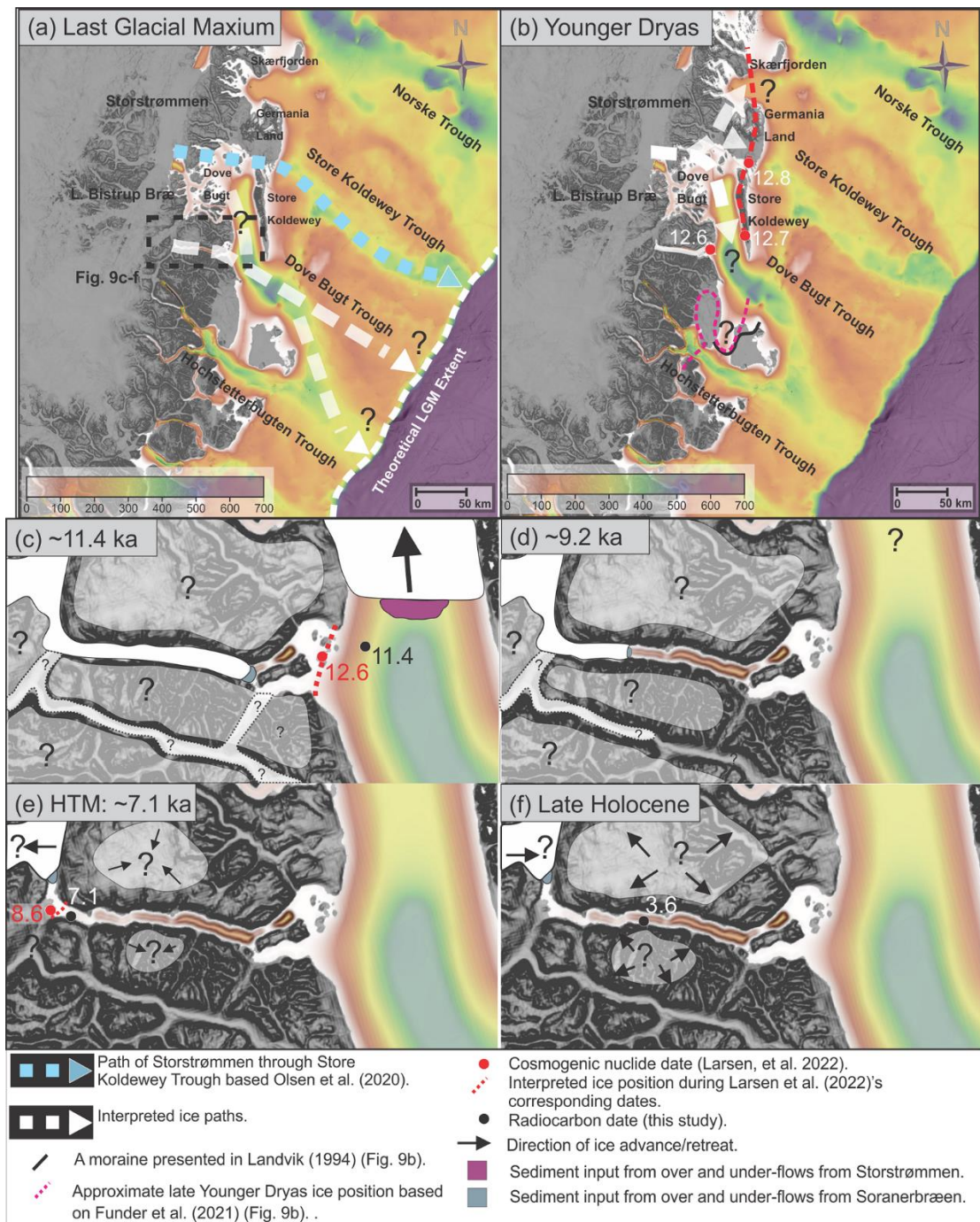
566 **5.1. *Ice Sheet advance***

567 The appearance of glacial lineations in Bessel Fjord suggest that the fjord was once fully
568 glaciated, which is in accordance with the inferred shelf break-terminating ice sheet inferred for
569 the LGM from other studies (e.g., Laberg et al., 2017; Olsen et al., 2020) (Figs. 9a & 9b). Ice
570 that filled the fjord is believed to most likely be from the modern Soranerbræen glacier but may
571 have also included ice caps and other nearby branches of inland ice.

572 Glacial lineations are believed to have formed during the LGM but could have also formed
573 during an ice readvance in the deglaciation (see below). Onshore and south of Bessel Fjord,
574 two sets of striations identified in Langsødalen (Hjort, 1979, 1981) may suggest that this valley
575 experienced two glaciation events (Fig. 1c). Striations, and lateral moraines, found along the
576 fjord axis may be the result of the east-west movement of ice through the valley, where SW
577 oriented striations may be the result of Storstrømmen encroaching also onto terrestrial areas.
578 Hjort (1981) suggested that striae on Haystack may indicate that ice flow was dominant from the
579 north during the Nanok Stadial but ice pressure from Langsødalen dominated later after
580 deglaciation begun. Thus, it is possible that ice masses drained through both Bessel Fjord and
581 Langsødalen during full-glacial conditions further advancing into Dove Bugt/Store Bælt.

582 In Store Bælt, the orientation of glacial lineations (e.g., MSGLs) suggest that ice flowed to the
583 south along the west coast of Store Koldewey, marking the southwards expansion of the
584 Storstrømmen ice stream (Figs. 9a & 9b). East of Dove Bugt, MSGLs identified in Store
585 Koldewey Trough are believed to have formed when the Storstrømmen ice stream acted as a
586 “pure” ice stream (Bentley, 1987; Stokes and Clark, 1999) and overrode the underlying
587 topography during the LGM (Fig. 9a; Olsen et al., 2020). It was theorized that at a later phase,
588 when the ice sheet began to thin, the ice stream became more influenced by the topography of
589 deep troughs, draining northwards to Jøkelbugten and southwards to Dove Bugt (Olsen et al.,
590 2020). Assuming these two phases occurred in the Storstrømmen ice stream development, it is
591 possible that these glacial lineations in Store Bælt represent a period when a branch of the ice
592 stream began conforming to topographical controls (e.g., Store Koldewey) and flowed towards
593 the south. At this point the ice may have flowed into the southeast through Dove Bugt Trough
594 (Fig. 9a).

595 An alternative interpretation, that cannot be excluded, is that these MSGLs formed during a
596 glacial re-advance that followed the LGM. Between Hochstetter Forland and Shannon Ø a
597 submerged moraine has been identified in Shannon Sound, which may indicate that at one point
598 the ice stream travelled south rather than through Dove Bugt Trough (Figs. 9b & 10a; Hjort,
599 1981; Landvik, 1994; Larsen et al., 2016; Funder et al., 2021). However, onshore deglaciation
600 ages in Store Koldewey, Germania Land and Trums Ø, do not support an ice advance during
601 the Younger Dryas (Fig. 10b; see below). This was possibly an ice readvance of the GrIS
602 outlet(s) (Soranerbræen, L. Bistrup Bræ and/or Storstrømmen) through western, inner Dove



603

604 *Figure 9. Maps showing ice sheet extent and advancement/retreat directions in SW Dove Bugt and Bessel Fjord*
 605 *during a range of periods. (a) The interpreted position of the ice sheet during the LGM. (b) The theoretical position of*
 606 *ice in Bessel Fjord and Dove Bugt during the Younger Dryas. (c) The ice position in Bessel Fjord at ~11.4 ka based*
 607 *on approximated deglaciation date presented in this study and the position and radiocarbon date for gravity core*
 608 *HH17-1309. The size of ice caps in c-f are only indicative. (d) The position of ice in Bessel Fjord at ~9.2 based on*
 609 *approximated deglaciation data from this study. (e) Ice retreating beyond our gravity core (HH17-1290) at ~7.1 ka*
 610 *during the HTM. (f) The Late Holocene ice expanse in Bessel Fjord with a radiocarbon date from gravity core HH17-*
 611 *1289. Background bathymetry displayed using IBCAO data (Jakobsson et al., 2020).*



612

613 *Figure 10. (a) Marine moraine ridges and glacial lineations from the current study together with previously mapped*
 614 *marine and terrestrial features. (b) Location of deglaciation dates from this study (Table 5) and previous publications.*
 615 *See Table 3 for recalibrated radiocarbon dates. H: Hjort Lake, D: Duck Lake. Background displayed using IBCAO*
 616 *data (Jakobsson et al., 2020).*

617 Bugt (Fig. 9b), where the surroundings (onshore and offshore) were not or less affected. If this
 618 is correct, the readvance may have occurred during the Younger Dryas (prior to 11.4 ka cal BP,
 619 see below).

620 5.2. Ice Sheet retreat through Store Bælt

621 The deglaciation age of 11.4 ka cal BP (Table 5) from Store Bælt immediately east of the Bessel
 622 fjord entrance is attributed to the retreat of a N-S bound branch of the NEGIS (Fig. 9c) due to
 623 the presence of N-S oriented glacial lineations near the gravity core. This date represents a
 624 minimum age for the deglaciation as it is not from the base of the deglacial deposits. Previously
 625 published dates constraining the timing of deglaciation in Dove Bugt have been restricted to
 626 terrestrial regions (Fig. 10b). Using cosmogenic nuclide dating, Skov et al., (2020) produced
 627 deglaciation ages of ca. 12.7 ka cal BP at Store Koldewey and ca. 9.8 ka cal BP at Pusterdal
 628 and later Larsen et al. (2022) produced a number of deglaciation ages across Dove Bugt and
 629 Bessel Fjord (8.6-12.8 ka cal BP) (Fig. 10b).

630 Our minimum age of ~11.4 ka cal BP from HH17-1309 largely matches findings in Dove Bugt
631 and Hochstetter Forland (Fig. 10b). It is slightly later than cosmogenic nuclide ages obtained
632 from Larsen et al. (2022) on Trums Ø (12.6 ka cal BP) and a Nanok moraine on southern Store
633 Koldewey (12.7 ka cal BP), but earlier than a second Store Koldewey Nanok moraine (11.0 ka
634 cal BP) as well as positions closer to the modern ice margin of Storstrømmen, such as Licht Ø
635 (10.8 ka cal BP) and Bræ Øerne (8.9 ka cal BP). Thus, Store Koldewey, and Trums Ø may have
636 been partially deglaciated slightly prior to the final retreat of the NEGIS through Store Bælt.

637 Radiocarbon dates obtained from lake sediments on Store Koldewey suggest that the earliest
638 onset of warmth may have begun ~10 ka cal BP (Klug et al., 2009), therefore, the deglaciation
639 of the area beginning prior to this may further support these results. Additionally, Landvik (1994)
640 produced a range of deglaciation ages between 9.6 to 8.5 ka cal BP along the northern coast of
641 Dove Bugt (Hvalrosodden and Snenæs on Germania Land) and Hjort (1981, 1979) provided a
642 range of deglaciation ages between 10.6 to 9.8 ka cal BP on Hochstetter Forland. Later Björck et
643 al. (1994), on Hochstetter Forland, dated *Hiatella arctica* shells near the shore of Peters Bugt
644 Sø and *Portlandia arctica* shells in a delta distal to a Nanok I ridge to 10.4 and 11.3 ka cal BP,
645 respectively (Table 3; Fig. 10b).

646 Although based on a limited data set, the lack of prominent morainal landforms in Store Bælt
647 may also suggest a rapid retreat through the region. A small number of retreat moraines have
648 been observed in an isolated region of the study area, but the most prominent geomorphic
649 landforms are glacial lineations. Placing Store Bælt within the context of Dowdeswell et al.
650 (2008)'s proposed model for ice streams in high latitudes, ice likely retreated through the area
651 rapidly, although the presence of small moraines may suggest brief periods of stagnation. This
652 is in accordance with findings by Larsen et al. (2020, 2022) that deep fjords and outer regions in
653 eastern North Greenland were rapidly deglaciated between ~12.6 and 10 ka cal BP. However,
654 additional data is required to confirm this.

655 Oceanic warming is believed to have contributed to the deglaciation of the inner shelf further
656 north and south of Dove Bugt (e.g., Jackson et al., 2022; Davies et al., 2022). Within the study
657 area, Store Koldewey does largely block oceanic water from the shelf from entering Store Bælt,
658 however, it is possible that warmer water traveled through the Dove Bugt Trough to the south
659 and impacted a north-south branch of the ice stream. This mechanism for warm water transport
660 has also been suggested for other east Greenland troughs (Arndt et al., 2015) and used to
661 explain how warm water has reached other outlets of the NEGIS (e.g., Zachariae Isstrøm via
662 the Norske Trough (Schaffer et al., 2017)).

663 5.3. *Ice Sheet retreat through Bessel Fjord*

664 Cosmogenic nuclide dates from Trums Ø suggest that the deglaciation of the outer fjord began
665 around 12.6 ka cal BP. Gravity core HH17-1290, collected from the inner fjord region, consists
666 of sediments that reflect an increasingly ice distal environment up core. One radiocarbon date
667 from the core provides a minimum age of ~7.1 ka cal BP for the deglaciation of Soranerbræen
668 and/or local ice caps from the inner fjord region (Table 5 & Fig. 9e). This date, however, is not
669 from the base of the deglacial deposits and therefore represents a minimum age for the
670 deglaciation of the inner fjord. New cosmogenic nuclide dates from Vandrepasset (onshore
671 innermost Bessel fjord area, connecting the fjord and the next valley to the south) provide an
672 age of 8.6 ka cal BP for the deglaciation of the innermost fjord area (Larsen et al., 2022),
673 confirming this interpretation. Our minimum age of 7.1 ka cal BP and the results of Larsen
674 (2022) falls within a modelled ice sheet extent by Lecavalier et al. (2014) which placed the

675 position of the ice sheet in the middle of Bessel Fjord at 9 ka cal BP and that the present-day ice
676 margin is reached by 6 ka cal BP. The minimum age also agrees with the onset of HTM on
677 Store Koldewey (~8.0 to 4.0 ka cal BP) (Wagner et al., 2008; Klug et al., 2009; Schmidt et al.,
678 2011) and Hochstetter Forland (8.8 and 5.6 ka cal BP) (Björck & Persson, 1981; Björck et al.,
679 1994). Thus, the GrIS retreated from the marine realm in early Holocene, slightly before or at
680 the time of the HTM in this region (characterized by a mean July temperature 2-3°C higher than
681 at present; Bennike et al., 2008).

682 The appearance of recessional moraines in Bessel Fjord suggests that the fjord underwent a
683 stepwise deglaciation. The large moraine identified between Basin 3 and Basin 4 (M3; Fig. 7e)
684 is believed to have formed during a major ice halt or readvance, possibly climatically induced.
685 Smaller moraines occasionally follow topographic boundaries, which may suggest that the
686 retreat of ice in Bessel Fjord was also partly topographically controlled. Recessional moraines
687 identified by Olsen et al (2020) east of Dove Bugt in Store Koldewey Trough contain similar
688 heights to those identified here (excluding M3). However, there are more moraines identified in
689 Store Koldey Trough than in Bessel Fjord, and they are wider, which is likely due to the lack of
690 topographic confinement.

691 A decrease in atmospheric temperatures in early Holocene is recorded in the Greenland
692 Summit temperature records and includes the Preboreal Oscillation, the 9.2 ka event, the Pre-
693 8.2 ka cooling, and the 8.2 ka event, with the 8.2 ka event being the largest hemispheric-wide
694 negative temperature excursion during the Holocene (Kobashi et al., 2017). We tentatively
695 suggest that some of the moraines identified in the Bessel fjord may have developed during
696 some of these events. From this we suggest that increased Northern Hemisphere summer
697 insolation that peaked in the early Holocene was the main control for this part of the deglaciation
698 during which the ice front receded from the coastline to the west of (onshore) Bessel Fjord, a
699 distance of ~60 km. Assuming that this occurred over a maximum period of ~4.3 ka cal BP
700 (11.4-7.1 ka cal BP, see discussion above on the timing and length of this period), this
701 corresponds to an average ice recession rate of ~14 m/yr. This rate, a minimum rate, is
702 considered realistic as it is half (or less) than the rate estimated from the Nioghalvfjærdsfjorden
703 further north (also part of the Storstrømmen ice stream) where a rate of ~30-40 m/yr was
704 reported (Bennike & Björck, 2002).

705 Applying this minimum rate to the distance between Trums Ø (Larsen, et al., (2022); 12.6 ka cal
706 BP) and the major mounds and moraines identified in this study (M1, M2, M3 & M6), yields the
707 approximate minimum ages of 11.4, 10.5, 9.7 and 9.2 ka, respectively. This places
708 Soranerbræen between large moraine M3 and the bedrock mound M6 around the 9.2 ka event
709 (Fig. 9d). This is noteworthy as M3, and other many of the smaller moraines identified between
710 these two features, may have formed during this climatically cooler period. Additionally, many
711 smaller moraines in the fjord follow topographic boundaries, which may suggest that the retreat
712 of ice in Bessel Fjord was partly topographically controlled.

713 While oceanic warming may be partially responsible for the retreat of the NEGIS through Store
714 Bælt, we believe that Bessel Fjord is too sheltered by the sill at its entrance to have allowed
715 warm, intermediate water to enter and make a significant impact of the deglaciation of the
716 southern outlet of Soranerbræen. Our bathymetric dataset reveals that the depth of the sill is
717 between ~50 to 200 m, however large parts of it are above water and form islands. This is far
718 shallower than other fjord sills in the region that are theorized to have blocked warm Atlantic
719 Water (e.g., the sill in Dijnphna Sund to the north, which has a maximum depth of 170 m

720 (Wilson and Straneo, 2015)). Also, the effect of the glacio-eustatic readjustment is considered to
721 be small for this region, ~9.5 m higher in the Young Sound region (slightly south of our study
722 area) 7500 years ago (Pedersen et al., 2011). Rignot et al. (2022) also theorized that seafloor
723 topography may impact whether warm water is reaching the northern outlet of Soranerbræen.
724 They suggested further that the grounding line retreat of Storstrømmen, L. Bistrup Bræ, and
725 possibly Soranerbræen, may primarily be caused by ice thinning from atmospheric warming
726 (Rignot et al., 2022). We suggest that a similar mechanism may be responsible for
727 Soranerbræen's retreat through Bessel fjord during the deglaciation.

728 5.4. *Holocene glacier variability and sedimentary processes in Dove Bugt*

729 Sedimentological evidence (e.g., laminated muds) from HH17-1309 suggests, that suspension
730 settling from a glacial source(s) likely dominated southwestern Dove Bugt during the Holocene.
731 The contribution of sediment from the NEGIS seems unlikely, as Pusterdal became deglaciated
732 by 9.5 ka cal BP (Skov et al., 2020) and Storstrømmen retreated beyond Bræ Øerne by 8.9 ka
733 cal BP (Larsen et al., 2022), therefore it very well may be from Soranerbræen, or local ice caps.

734 During the latter part of the HTM in the middle Holocene, a time period in which some glaciers
735 are believed to have reached their minimum extent across Greenland, the NEGIS is believed to
736 have retreated beyond its current position between 5.4 to 1.2 ka cal BP (Table 3), creating the
737 Storstrømmen Sound (Weidick et al., 1994). Relating the core sedimentology to a linear age
738 model developed from sedimentation rates (i.e., Table 5), laminations appear less frequently in
739 core HH17-1309 during this period, yet they are not absent. Laminations are entirely absent in
740 the Bessel Fjord core HH17-1290 during this period and remain absent through the colder Late
741 Holocene. Later, during the Little Ice Age, Storstrømmen demonstrated to have expanded to its
742 modern day position (Weidick et al., 1994).

743 Gravity core HH17-1289, collected to the north of an onshore glaciofluvial channel connected to
744 a modern-day ice cap, transitions to complex assortment of sand layers just prior to 3,596 cal yr
745 BP (Fig. 7). Sedimentological evidence suggests that these sand layers are largely the result of
746 rapid, short lived depositional events (i.e., turbidity currents) interpreted to be related to the
747 growth of a delta slightly south of the core site, from glaciofluvial sediment input from a nearby
748 outlet glacier.

749 Pollen assemblage data from Hochstetter Forland mark the end of the HTM at 5.6 yr BP (Björck
750 and Persson, 1981; Björck et al., 1994) and information derived from aquatic organisms mark
751 the end of the HTM on Store Koldewey at 4 yr BP (Wagner et al., 2008; Klug et al., 2009b;
752 Schmidt et al., 2011). This coincides with the onset of turbidites in core HH17-1289. Therefore,
753 it is possible that this shift to sand dominated sedimentation within this core was controlled by
754 climatically driven processes. This onset is here suggested to result from higher sediment input
755 through the channel as local ice caps expanded outwards following the HTM, possibly in
756 response to this climate cooling (Fig. 9f). This period of cooling also corresponds to extended
757 concentrations of sea ice on the shelf (Kolling et al., 2017).

758 6. Conclusion

759 In summary:

- 760 • Glacial lineations (MSGLs) identified in SW Dove Bugt suggest fast-flowing ice,
761 interpreted to be from the NEGIS, developed during the LGM or an ice readvance during
762 the deglaciation.

- 763 • Our minimum deglaciation date for Store Bælt (>11.4 ka cal BP) is slightly later than
764 new cosmogenic nuclide dates found onshore on Trums Ø and one of two Nanok
765 stadials on Store Koldewey (Larsen et al., 2022) as well as various other dates across
766 Store Koldewey (e.g., Skov et al., 2020). Thus, Store Koldewey and Trums Ø may have
767 been partially deglaciated prior to the final retreat of the NEGIS through Store Bælt.
- 768 • Moraines in Bessel Fjord (to the west of Dove Bugt) suggests that the fjord underwent
769 multiple halts/or readvances upon deglaciation. Thus, the bathymetry of Bessel Fjord
770 indicates that the glacial dynamics of the fjord were more dynamic than onshore
771 evidence suggests.
- 772 • The radiocarbon date of 7.1 ka cal BP obtained in an inner fjord core is interpreted as a
773 minimum age at which Soranerbræen retreated to or beyond its present-day onshore
774 position west of the fjord and is in conformity with cosmogenic nuclide dates presented
775 by Larsen et al. (2022) in the onshore inner fjord (8.6 ka cal BP).
- 776 • Ice recession in Bessel Fjord occurred at a minimum average rate of ~14 m/yr.
- 777 • The GrlS retreated from the marine realm in the early Holocene, around the time of the
778 onset of the HTM in this region. From this we suggest that increased Northern
779 Hemisphere summer insolation that peaked in the early Holocene was the main control
780 for this part of the deglaciation.
- 781 • A low sedimentation rate of 13.63 cm/ka after 7.1 ka cal BP in HH17-1289, and the
782 presence of only massive mud, suggests that Soranerbræen did not expand back into
783 Bessel Fjord for the remainder of the Holocene.
- 784 • The transition of mud to muddy sand at 4 ka cal BP in a mid-fjord core HH17-1289 may
785 provide evidence for local ice cap growth. Thus, ice caps in Bessel Fjord may have
786 fluctuated with greater sensitivity to climatic conditions than the NE sector of the GrlS
787 during the cooling phase that followed the HTM.

788

789 *Data availability:* The bathymetry and core data from UiT The Arctic University of Norway will be
790 available upon reasonable request at UiT's open research data repository:
791 <https://dataverse.no/dataverse/uit>.

792 *Author contributions:* Jan Sverre Laberg and Tom Arne Rydningen designed this study and
793 collected the new data during the 2017 TUNU VII cruise. The bathymetrical and lithological data
794 were interpreted by Kevin Zoller in collaboration with Jan Sverre Laberg and Tom Arne
795 Rydningen. Kevin Zoller prepared the manuscript with contributions from all co-authors.

796 *Competing interests:* The authors declare that they have no conflict of interest.

797 *Acknowledgement:* We would like to thank the participants of the 2017 TUNU cruise to
798 Greenland for making this project possible. A special thanks to the captain and crew of the RV
799 *Helmer Hanssen* for their involvement in the cruise and assistance in collecting the data. A
800 thanks also goes out to the lab staff at UiT, Trine Dahl, Karina Monsen and Ingvild Hald, who
801 assisted with processing sediment core samples for this project. We would also like to thank
802 Gesine Mollenhauer and the lab staff at the Alfred Wegener Institut for providing us with
803 radiocarbon dated material using their MICADAS. Funding for this work was provided by UiT
804 The Arctic University of Norway.

805

806 References

- 807 Arndt, J. E.: Marine geomorphological record of Ice Sheet development in East Greenland since
808 the Last Glacial Maximum, *J. Quat. Sci.*, 33, 853–864, <https://doi.org/10.1002/jqs.3065>, 2018.
- 809 Arndt, J. E., Jokat, W., Dorschel, B., Mykleburst, R., Dowdeswell, J. A., and Evans, J.: A new
810 bathymetry of the Northeast Greenland continental shelf: Constraints on glacial and other
811 processes, *AGU Publ. Geochemistry Geophys. Geosystems*, 16, 267–300,
812 <https://doi.org/10.1002/2014GC005684.Key>, 2015.
- 813 Arndt, J. E., Jokat, W., and Dorschel, B.: The last glaciation and deglaciation of the Northeast
814 Greenland continental shelf revealed by hydro-acoustic data, *Quat. Sci. Rev.*, 160, 45–56, 2017.
- 815 Batchelor, C. L., Dowdeswell, J. A., and Rignot, E.: Submarine landforms reveal varying rates
816 and styles of deglaciation in North-West Greenland fjords, *Mar. Geol.*, 402, 60–80,
817 <https://doi.org/10.1016/j.margeo.2017.08.003>, 2018.
- 818 Bennike, O. and Björck, S.: Chronology of the last recession of the Greenland Ice Sheet, *J.*
819 *Quat. Sci.*, 17, 211–219, <https://doi.org/10.1002/jqs.670>, 2002.
- 820 Bennike, O. and Weidick, A.: Late Quaternary history around Nioghalvfjærdsfjorden and
821 Jøkelbugten, North-East Greenland, *Boreas*, 30, 205–227, <https://doi.org/10.1111/j.1502-3885.2001.tb01223.x>, 2001.
- 823 Bennike, O., Sørensen, M., Fredskild, B., Jacobsen, B. H., Böcher, J., Amsinck, S. L.,
824 Jeppesen, E., Andreasen, C., Christiansen, H. H., and Humlum, O.: Late Quaternary
825 Environmental and Cultural Changes in the Wollaston Forland Region, Northeast Greenland,
826 *Adv. Ecol. Res.*, 40, 45–79, [https://doi.org/10.1016/S0065-2504\(07\)00003-7](https://doi.org/10.1016/S0065-2504(07)00003-7), 2008.
- 827 Bentley, C. R.: Antarctic ice streams: a review, *Geophys. Res.*, 92(6), 8843–8858, 1987.
- 828 Biette, M., Jomelli, V., Chenet, M., Braucher, R., Rinterknecht, V., and Lane, T.: Mountain
829 glacier fluctuations during the Lateglacial and Holocene on Clavering Island (northeastern
830 Greenland) from ¹⁰Be moraine dating, *Boreas*, 49, 873–885, <https://doi.org/10.1111/bor.12460>,
831 2020.
- 832 Björck, S. and Persson, T.: Late Weichselian and Flandrian biostratigraphy and chronology from
833 hochstetter forland, northeast Greenland, *Medd. Om. Grøn. Geosci.*, 5, 1–19, 1981.
- 834 Björck, S., Wohlfarth, B., Bennike, O., Hjort, C., and Persson, T.: Revision of the early Holocene
835 lake sediment based chronology and event stratigraphy on Hochstetter Forland, NE Greenland,
836 *Boreas*, 23, 513–523, <https://doi.org/10.1111/j.1502-3885.1994.tb00619.x>, 1994.
- 837 Boulton, G. S. and Deynoux, M.: Sedimentation in glacial environments and the identification of
838 tills and tillites in ancient sedimentary sequences, *Precambrian Res.*, 15, 397–422,
839 [https://doi.org/10.1016/0301-9268\(81\)90059-0](https://doi.org/10.1016/0301-9268(81)90059-0), 1981.
- 840 Boulton, G. S., Hagdorn, M., and Hulton, N. R. J.: Streaming flow in an ice sheet through a
841 glacial cycle, *Ann. Glaciol.*, 36, 117–128, <https://doi.org/10.3189/172756403781816293>, 2003.
- 842 Briner, J. P., McKay, N. P., Axford, Y., Bennike, O., Bradley, R. S., de Vernal, A., Fisher, D.,
843 Francus, P., Fréchette, B., Gajewski, K., Jennings, A., Kaufman, D. S., Miller, G., Rouston, C.,
844 and Wagner, B.: Holocene climate change in Arctic Canada and Greenland, *Quat. Sci. Rev.*,
845 147, 340–364, <https://doi.org/10.1016/j.quascirev.2016.02.010>, 2016.
- 846 Cartigny, M. J. B., Postma, G., Berg, J. H., and Mastbergen, D. R.: A comparative study of

847 sediment waves and cyclic steps based on geometries, internal structures and numerical
848 modeling, *Mar. Geol.*, 280, 40–56, 2011.

849 Christiansen, J. S.: The TUNU-Programme : Euro-Arctic Marine Fishes — Diversity and
850 Adaptation, in: *Adaptation and Evolution in Marine Environments*, vol. 1, 35–50,
851 <https://doi.org/10.1007/978-3-642-27352-0>, 2012.

852 Clark, C. D.: Mega-scale lineations and cross-cutting ice-flow landforms, *Earth Surf. Process.*
853 *Landforms*, 18, 1–29, 1993.

854 Clark, C. D. and Stokes, C. R.: Palaeo-ice stream landsystem, in: *Glacial Landscapes*, edited
855 by: Evans, D. J. A., Edward Arnold, London, 204–227, 2003.

856 Clark, C. D., Tulaczyk, S. M., Stokes, C. R., and Canals, M.: A groove-ploughing theory for the
857 production of mega-scale glacial lineations, and implications for ice-stream mechanics, *J.*
858 *Glaciol.*, 49, 240–256, <https://doi.org/10.3189/172756503781830719>, 2003.

859 Cohen, J., Screen, J. A., Furtado, J. C., Barlow, M., Whittleston, D., Coumou, D., Francis, J.,
860 Dethloff, K., Entekhabi, D., Overland, J., and Jones, J.: Recent Arctic amplification and extreme
861 mid-latitude weather, *Nat. Publ. Gr.*, 7, 627–637, <https://doi.org/10.1038/ngeo2234>, 2014.

862 Cowan, E. A., Seramur, K. C., Cai, J., and Powell, R. D.: Cyclic sedimentation produced by
863 fluctuations in meltwater discharge, tides and marine productivity in an Alaskan fjord,
864 *Sedimentology*, 46, 1109–1126, <https://doi.org/10.1046/j.1365-3091.1999.00267.x>, 1999.

865 Cremer, H., Bennike, O., and Wagner, B.: Lake sediment evidence for the last deglaciation of
866 eastern Greenland, *Quat. Sci. Rev.*, 27, 312–319,
867 <https://doi.org/10.1016/j.quascirev.2007.09.004>, 2008.

868 Davies, J., Mathiasen, A. M., Kristiansen, K., Hansen, K. E., Wacker, L., Alstrup, A. K. O., Munk,
869 O. L., Pearce, C., and Seidenkrantz, M. S.: Linkages between ocean circulation and the
870 Northeast Greenland Ice Stream in the Early Holocene, *Quat. Sci. Rev.*, 286, 107530,
871 <https://doi.org/10.1016/j.quascirev.2022.107530>, 2022.

872 Dowdeswell, J. A., Ottesen, D., Evans, J., Cofaigh, C. Ó., and Anderson, J. B.: Submarine
873 glacial landforms and rates of ice-stream collapse, *Geology*, 36, 819–822,
874 <https://doi.org/10.1130/G24808A.1>, 2008.

875 Dowdeswell, J. A., Hogan, K. A., Ó Cofaigh, C., Fugelli, E. M. G., Evans, J., and Noormets, R.:
876 Late Quaternary ice flow in a West Greenland fjord and cross-shelf trough system: submarine
877 landforms from Rink Isbrae to Uummannaq shelf and slope, *Quat. Sci. Rev.*, 92, 292–309,
878 2014.

879 Dowdeswell, J. A., Canals, M., Jakobsson, M., Todd, B. J., Dowdeswell, E. K., and Hogan, K.
880 A.: The variety and distribution of submarine glacial landforms and implications for ice-sheet
881 reconstruction, *Geol. Soc. Mem.*, 46, 519–552, <https://doi.org/10.1144/M46.183>, 2016.

882 Evans, J., Dowdeswell, J. A., Grobe, H., Niessen, F., Stein, R., Hubberten, H. W., and
883 Whittington, R. J.: Late Quaternary sedimentation in Kejser Franz Joseph Fjord and the
884 continental margin of East Greenland, *Geol. Soc. Spec. Publ.*, 203, 149–179,
885 <https://doi.org/10.1144/GSL.SP.2002.203.01.09>, 2002.

886 Evans, J., Ó Cofaigh, C., Dowdeswell, J. A., and Wadhams, P.: Marine geophysical evidence
887 for former expansion and flow of the Greenland Ice Sheet across the north-east Greenland
888 continental shelf, *J. Quat. Sci.*, 24, 279–293, 2009.

- 889 Eyles, N., Eyles, C. H., and Niall, An. D.: Lithofacies types and vertical profile models; an
890 alternative approach to the description and environmental interpretation of glacial diamict and
891 diamictite sequences, *Sedimentology*, 30, 393–410, 1983.
- 892 Folk, R. L.: The Distinction between Grain Size and Mineral Composition in Sedimentary-Rock
893 Nomenclature, *J. Geol.*, 62, 344–359, 1954.
- 894 Folk, R. L. and Ward, W.: Brazos river bar, a study in the significance of grain size parameters.,
895 *J. Sediment. Petrol.*, 27, 34–59, 1957.
- 896 Forwick, M. and Vorren, T. O.: Deglaciation history and post-glacial mass movements in
897 Balsfjord, northern Norway, *Polar Res.*, 21(2), 259–266, 1998.
- 898 Forwick, M. and Vorren, T. O.: Late Weichselian and Holocene sedimentary environments and
899 ice rafting, *Palaeogeogr. Palaeoclimatol. Palaeoecol.*, 280, 258–274, 2009.
- 900 Forwick, M., Vorren, T. O., Hald, M., Korsun, S., Roh, Y., Vogt, C., and Yoo, K. C.: Spatial and
901 temporal influence of glaciers and rivers on the sedimentary environment in Sassenfjorden and
902 Tempelfjorden, Spitsbergen, *Geol. Soc. London, Spec. Publ.*, 344, 163–193,
903 <https://doi.org/10.1144/SP344.13>, 2010.
- 904 Funder, S., Kjeldsen, K. K., Kjær, H. K., and Ó Cofaigh, C.: The Greenland Ice Sheet During the
905 Past 300,000 Years: A Review, *Dev. Quat. Sci.*, 15, 699–713, <https://doi.org/10.1016/B978-0-444-53447-7.00050-7>, 2011.
- 907 Funder, S., Sørensen, A. H. L., Larsen, N. K., Bjørk, A. A., Briner, J. P., Olsen, J., Schomacker,
908 A., Levy, L. B., and Kjær, K. H.: Younger Dryas ice margin retreat in Greenland: new evidence
909 from southwestern Greenland, *Clim. Past*, 17, 587–601, 2021.
- 910 Geirsdóttir, Á., Hardardóttir, J., and Andrews, J. T.: Late-Holocene terrestrial glacial history of
911 Miki and I.C. Jacobsen Fjords, East Greenland, *Holocene*, 10, 123–134,
912 <https://doi.org/10.1191/095968300666213169>, 2000.
- 913 Håkansson, L., Graf, A., Strasky, S., Ivy-ochs, S., Kubik, P. W., Hjort, C., Shluchter, C.,
914 Geografiska, S., Series, A., Geography, P., Hakansson, L., Graf, A., Strasky, S., Ivy-ochs, S.,
915 Kubik, P. W., Hjort, C., and Schlichter, C.: Cosmogenic ¹⁰Be-Ages from the Store Koldewey
916 Island, NE Greenland, *Geogr. Ann. Ser. A Phys. Geogr.*, 89, 195–202, 2007.
- 917 Hansen, K. E., Lorenzen, J., Davies, J., Wacker, L., Pearce, C., and Seidenkrantz, M.-S.:
918 Deglacial to Mid Holocene environmental conditions on the northeastern Greenland shelf,
919 *Quaternary Sci. Rev.*, 293, 107704, 2022.
- 920 Heaton, T. J., Köhler, P., Butzin, M., Bard, E., Reimer, R. W., Austin, W. E. N., Ramsey, C. B.,
921 Grootes, P. M., Hughen, K. A., Kromer, B., Reimer, P. J., and Heaton, T. J.: Marine20 — The
922 Marine Radiocarbon Age Calibration Curve (0-55,000 CAL BP), *Radio*, 62, 779–820,
923 <https://doi.org/10.1017/RDC.2020.68>, 2020.
- 924 Heaton, T. J., Bard, E., Ramsey, C. B., Butzin, M., Hatté, C., Hughen, K. A., Köhler, P., and
925 Reimer, P. J.: A Response to Community Questions on the Marine20 Radiocarbon Age
926 Calibration Curve: Marine Reservoir Ages and The Calibration of ¹⁴C Samples from the
927 Oceans, *Radiocarbon*, 65, 247–273, <https://doi.org/10.1017/RDC.2022.66>, 2022.
- 928 Higgins, A. K.: North Greenland Glaciers Velocities and Calf Ice Production, *Polarforschung*, 60,
929 1–23, 1991.
- 930 Hill, P. R.: Changes in submarine channel morphology and strata development from repeat

- 931 multibeam surveys in the Fraser River delta, western Canada, in: *Sediments, Morphology and*
932 *Sedimentary Processes on Continental Shelves*, edited by: Li, M. Z., Sherwood, C. R., and Hill,
933 P. R., Blackwell Science, International Association of Sedimentologists, 47–70, 2012.
- 934 Hjort, C.: Glaciation in northern East Greenland during the Late Weichselian and Early
935 Flandrian, *Boreas*, 8, 281–296, <https://doi.org/10.1111/j.1502-3885.1979.tb00812.x>, 1979.
- 936 Hjort, C.: A glacial chronology for northern East Greenland, *Boreas*, 10, 259–274, 1981.
- 937 Hjort, C. and Björck, S.: A re-evaluated glacial chronology for Northern East Greenland, *Geol.*
938 *Föreningen i Stock. Förhandlingar*, 105, 235–243, <https://doi.org/10.1080/11035898309452590>,
939 1983.
- 940 Hogan, K. A., Dowdeswell, J. A., Noormets, R., Evans, J., and Ó Cofaigh, C.: Evidence for full-
941 glacial flow and retreat of the Late Weichselian Ice Sheet from the waters around Kong Karls
942 Land, eastern Svalbard, *Quat. Sci. Rev.*, 29, 3563–3582,
943 <https://doi.org/10.1016/j.quascirev.2010.05.026>, 2010.
- 944 Hogan, K. A., Ó Cofaigh, C., Jennings, A. E., Dowdeswell, J. A., and Hiemstra, J. F.:
945 Deglaciation of a major palaeo-ice stream in Disko Trough, West Greenland, *Quat. Sci. Rev.*,
946 147, 5–26, 2016.
- 947 Huddart, D. and Lister, H.: The Origin of Ice Marginal Terraces and Contact Ridges of East
948 Kangerdluarssuk Glacier, SW Greenland, *Geogr. Ann.*, 63 A, 31–39, 1981.
- 949 Jackson, R., Andreasen, N., Oksman, M., Andersen, T. J., Pearce, C., Seidenkrantz, M.-S., and
950 Ribeiro, S.: Marine conditions and development of the Sirius Water polynya on the North-East
951 Greenland shelf during the Younger Dryas-Holocene, *Quat. Sci. Rev.*, 291, 107647, 2022.
- 952 Jakobsson, M., Hogan, K. A., Mayer, L. A., Mix, A., Jennings, A., Stoner, J., Eriksson, B.,
953 Jerram, K., Mohammad, R., Pearce, C., Reilly, B., and Stranne, C.: The Holocene retreat
954 dynamics and stability of Petermann Glacier in northwest Greenland, *Nat. Commun.*, 9,
955 <https://doi.org/10.1038/s41467-018-04573-2>, 2018.
- 956 Jakobsson, M., Mayer, L. A., Bringensparr, C., Castro, C. F., Mohammad, R., Johnson, P.,
957 Ketter, T., Accettella, D., Amblas, D., An, L., Arndt, J. E., Canals, M., Casamor, J. L., Chauché,
958 N., Coakley, B., Danielson, S., Demarte, M., Dickson, M. L., Dorschel, B., Dowdeswell, J. A.,
959 Dreutter, S., Fremand, A. C., Gallant, D., Hall, J. K., Hehemann, L., Hodnesdal, H., Hong, J.,
960 Ivaldi, R., Kane, E., Klaucke, I., Krawczyk, D. W., Kristoffersen, Y., Kuipers, B. R., Millan, R.,
961 Masetti, G., Morlighem, M., Noormets, R., Prescott, M. M., Rebesco, M., Rignot, E., Semiletov,
962 I., Tate, A. J., Travaglini, P., Velicogna, I., Weatherall, P., Weinrebe, W., Willis, J. K., Wood, M.,
963 Zarayskaya, Y., Zhang, T., Zimmermann, M., and Zinglensen, K. B.: The International
964 Bathymetric Chart of the Arctic Ocean Version 4.0, *Sci. Data*, 7, 1–14,
965 <https://doi.org/10.1038/s41597-020-0520-9>, 2020.
- 966 Joughin, I., Fahnestock, M., MacAyeal, D., Bamber, J. L., and Gogineni, P.: Observation and
967 analysis of ice flow in the largest Greenland ice stream, *J. Geophys. Res. Atmos.*, 106, 34021–
968 34034, <https://doi.org/10.1029/2001JD900087>, 2001.
- 969 Kelly, M. A., Lowell, T. V., Hall, B. L., Schaefer, J. M., Finkel, R. C., Goehring, B. M., Alley, R.
970 B., and Denton, G. H.: A ^{10}Be chronology of lateglacial and Holocene mountain glaciation in the
971 Scoresby Sund region, east Greenland: implications for seasonality during lateglacial time,
972 *Quat. Sci. Rev.*, 27, 2273–2282, 2008.
- 973 Kempf, P., Forwick, M., Laberg, J. S., and Vorren, T. O.: Late Weichselian and Holocene

974 sedimentary palaeoenvironment and glacial activity in the high-arctic van Keulenfjorden,
975 Spitsbergen, *The Holocene*, 23 (11), 1607–1618, <https://doi.org/10.1177/0959683613499055>,
976 2013.

977 Khan, S. A., Kjær, K. H., Bevis, M., Bamber, J. L., Wahr, J., Kjeldsen, K. K., Bjørk, A. A.,
978 Korsgaard, N. J., Stearns, L. A., Van Den Broeke, M. R., Liu, L., Larsen, N. K., and Muresan, I.
979 S.: Sustained mass loss of the northeast Greenland ice sheet triggered by regional warming,
980 *Nat. Clim. Chang.*, 4, 292–299, <https://doi.org/10.1038/nclimate2161>, 2014.

981 King, E. C., Hindmarsh, R. C. A., and Stokes, C. R.: Formation of mega-scale glacial lineations
982 observed beneath a West Antarctic ice stream, *Nat. Geosci.*, 2, 585–588,
983 <https://doi.org/10.1038/ngeo581>, 2009.

984 King, M. D., Howat, I. M., Candela, S. G., Noh, M. J., Jeong, S., Noël, B. P. Y., van den Broeke,
985 M. R., Wouters, B., and Negrete, A.: Dynamic ice loss from the Greenland Ice Sheet driven by
986 sustained glacier retreat, *Commun. Earth Environ.*, 1, 1–7, [https://doi.org/10.1038/s43247-020-](https://doi.org/10.1038/s43247-020-0001-2)
987 0001-2, 2020.

988 Klages, J. P., Kuhn, G., Hillenbrand, C.-D., Graham, A. G. C., Smith, J. A., Larter, R. D., and
989 Gohl, K.: First geomorphological record and glacial history of an inter-ice stream ridge on the
990 West Antarctic continental shelf, *Quat. Sci. Rev.*, 61, 47–61, 2013.

991 Klages, J. P., Kuhn, G., Graham, A. G. C., Hillenbrand, C.-D., Smith, J. A., Nitsche, F. O.,
992 Larter, R. D., and Gohl, K.: Palaeo-ice stream pathways and retreat style in the easternmost
993 Amundsen Sea Embayment, West Antarctica, revealed by combined multibeam bathymetric
994 and seismic data, *Geomorphology*, 245, 207–222, 2015.

995 Klug, M., Schmidt, S., Melles, M., Wagner, B., Bennike, O., and Heiri, O.: Lake sediments from
996 Store Koldewey, Northeast Greenland, as archive of Late Pleistocene and Holocene climatic
997 and environmental changes, *Boreas*, 38, 59–71, [https://doi.org/10.1111/j.1502-](https://doi.org/10.1111/j.1502-3885.2008.00038.x)
998 3885.2008.00038.x, 2009a.

999 Klug, M., Bennike, O., and Wagner, B.: Repeated short-term bioproductivity changes in a
1000 coastal lake on Store Koldewey, northeast Greenland: An indicator of varying sea-ice
1001 coverage?, *Holocene*, 19, 653–663, <https://doi.org/10.1177/0959683609104040>, 2009b.

1002 Klug, M., Bennike, O., and Wagner, B.: Late Pleistocene to early Holocene environmental
1003 changes on Store Koldewey, coastal north-east Greenland, *Polar Res.*, 35,
1004 <https://doi.org/10.3402/polar.v35.21912>, 2016.

1005 Kobashi, T., Menviel, L., Jeltsch-Thömmes, A., Vinther, B. M., Box, J. E., Muscheler, R.,
1006 Nakaegawa, T., Pfister, P. L., Döring, M., Leuenberger, M., Wanner, H., and Ohmura, A.:
1007 Volcanic influence on centennial to millennial Holocene Greenland temperature change, *Sci.*
1008 *Rep.*, 7, 1–10, <https://doi.org/10.1038/s41598-017-01451-7>, 2017.

1009 Kolling, H. M., Stein, R., Fahl, K., Perner, K., and Moros, M.: Short-term variability in late
1010 Holocene sea ice cover on the East Greenland Shelf and its driving mechanisms, *Palaeogeogr.*
1011 *Palaeoclimatol. Palaeoecol.*, 485, 336–350, <https://doi.org/10.1016/j.palaeo.2017.06.024>, 2017.

1012 Krieger, L., Floricioiu, D., and Neckel, N.: Drainage basin delineation for outlet glaciers of
1013 Northeast Greenland based on Sentinel-1 ice velocities and TanDEM-X elevations, *Remote*
1014 *Sens. Environ.*, 237, 111483, <https://doi.org/10.1016/j.rse.2019.111483>, 2020.

1015 Laberg, J. S., Forwick, M., and Husum, K.: New geophysical evidence for a revised maximum
1016 position of part of the NE sector of the Greenland ice sheet during the last glacial maximum,

- 1017 Arktos, 3, <https://doi.org/10.1007/s41063-017-0029-4>, 2017.
- 1018 Lambeck, K., Rouby, H., Purcell, A., Sun, Y., and Sambridge, M.: Sea level and global ice
1019 volumes from the Last Glacial Maximum to the Holocene, *Proc. Natl. Acad. Sci.*, 111, 15296–
1020 15303, <https://doi.org/10.1073/pnas.1411762111>, 2014.
- 1021 Landvik, J. Y.: The last glaciation of Germania Land and adjacent areas, northeast Greenland,
1022 *J. Quat. Sci.*, 9, 81–92, <https://doi.org/10.1002/jqs.3390090108>, 1994.
- 1023 Lane, T. P., Roberts, D. H., Ó Cofaigh, C., Vieli, A., and Moreton, S. G.: The glacial history of
1024 the southern Svartenhuk Halvø, West Greenland, *Arktos*, 1, 1–28,
1025 <https://doi.org/10.1007/s41063-015-0017-5>, 2015.
- 1026 Larsen, N. K., Funder, S., Linge, H., Möller, P., Schomacker, A., Fabel, D., Xu, S., and Kjær, K.
1027 H.: A Younger Dryas re-advance of local glaciers in north Greenland, *Quat. Sci. Rev.*, 147, 47–
1028 58, <https://doi.org/10.1016/j.quascirev.2015.10.036>, 2016.
- 1029 Larsen, N. K., Levy, L. B., Carlson, A. E., Buizert, C., Olsen, J., Strunk, A., Bjørk, A. A., and
1030 Skov, D. S.: Instability of the Northeast Greenland Ice Stream over the last 45,000 years, *Nat.*
1031 *Commun.*, 9, 3–10, <https://doi.org/10.1038/s41467-018-04312-7>, 2018.
- 1032 Larsen, N. K., Søndergaard, A. S., Levy, L. B., Olsen, J., Strunk, A., Bjørk, A. A., and Skov, D.:
1033 Contrasting modes of deglaciation between fjords and inter-fjord areas in eastern North
1034 Greenland, *Boreas*, 49, 905–919, <https://doi.org/10.1111/bor.12475>, 2020.
- 1035 Larsen, N. K., Søndergaard, A. S., Levy, L. B., Strunk, A., Skov, D. S., Bjørk, A., Khan, S. A.,
1036 and Olsen, J.: Late glacial and Holocene glaciation history of North and Northeast Greenland,
1037 *Arctic, Antarct. Alp. Res.*, 54, 294–313, <https://doi.org/10.1080/15230430.2022.2094607>, 2022.
- 1038 Levy, L. B., Kelly, M. A., Lowell, T. V., Hall, B. L., Howley, J. A., and Smith, C. A.: Coeval
1039 fluctuations of the Greenland ice sheet and a local glacier, central East Greenland, during late
1040 glacial and early Holocene time, *Geophys. Res. Lett.*, 43, 1623–1631, 2016.
- 1041 Lyså, A. and Vorren, T. O.: Seismic facies and architecture of ice-contact submarine fans in
1042 high-relief fjords, Troms, Northern Norway, *Boreas*, 26, 309–328, 1997.
- 1043 Mouginot, J., Rignot, E., Scheuchl, B., Fenty, I., Khazendar, A., Morlighem, M., Buzzi, A., and
1044 Paden, J.: Fast retreat of Zachariae Isstrom, Northeast Greenland, *Science (80-.)*, 350, 1357–
1045 1361, 2015.
- 1046 Mouginot, J., Bjørk, A. A., Millan, R., Scheuchl, B., and Rignot, E.: Insights on the Surge
1047 Behavior of Storstrømmen and L. Bistrup Bræ, Northeast Greenland, Over the Last Century,
1048 *Geophys. Res. Lett.*, 45, 11,197-11,205, <https://doi.org/10.1029/2018GL079052>, 2018.
- 1049 Newton, A. M. W., Knutz, P. C., Huse, M., Gannon, P., Brocklehurst, S. H., Clausen, O. R.,
1050 and Gong, Y.: Ice stream reorganization and glacial retreat on the northwest Greenland shelf,
1051 *Geophys. Res. Lett.*, 44, 7826–7835, <https://doi.org/10.1002/2017GL073690>, 2017.
- 1052 Ó Cofaigh, C.: Flow Dynamics and till genesis associated with a marin-based Antarctic palaeo-
1053 ice stream, *Quat. Sci. Rev.*, 24, 709–740, 2005.
- 1054 Ó Cofaigh, C., Dowdeswell, J. A., and Grobe, H.: Holocene glacimarine sedimentation, inner
1055 Scoresby Sund, East Greenland: The influence of fast-flowing ice-sheet outlet glaciers, *Mar.*
1056 *Geol.*, 175, 103–129, [https://doi.org/10.1016/S0025-3227\(01\)00117-7](https://doi.org/10.1016/S0025-3227(01)00117-7), 2001.
- 1057 Ó Cofaigh, C., Dowdeswell, J. A., Jennings, A. E., Hogan, K. A., Kilfeather, A., Hiemstra, J. F.,

- 1058 Noormets, R., Evans, J., McCarthy, D. J., Andrews, J. T., Lloyd, J. M., and Moros, M.: An
 1059 extensive and dynamic ice sheet on the west Greenland shelf during the last glacial cycle,
 1060 *Geology*, 41, 219–222, <https://doi.org/10.1130/G33759.1>, 2013.
- 1061 Olsen, I. L., Forwick, M., Laberg, J. S., and Rydningen, T. A.: Last Glacial ice-sheet dynamics
 1062 offshore NE Greenland – a case study from Store Koldewey Trough, *The Cryosphere*
 1063 *Discussions*, 2020.
- 1064 Olsen, I. L., Laberg, J. S., Forwick, M., Rydningen, T. A., and Husum, K.: Late Weichselian and
 1065 Holocene behavior of the Greenland Ice Sheet in the Kejser Franz Josef Fjord system, NE
 1066 Greenland, *Quat. Sci. Rev.*, 2022.
- 1067 Ottesen, D., Dowdeswell, J. A., Benn, D. I., Kristensen, L., Christiansen, H. H., Christensen, O.,
 1068 Hansen, L., Lebesbye, E., Forwick, M., and Vorren, T. O.: Submarine landforms characteristic of
 1069 glacier surges in two spitsbergen fjords, *Quat. Sci. Rev.*, 27, 1583–1599, 2008.
- 1070 Pados-Dibattista, T., Pearce, C., Detlef, H., Bendtsen, J., and Seidenkrantz, M. S.: Holocene
 1071 palaeoceanography of the Northeast Greenland shelf, *Clim. Past*, 18, 103–127,
 1072 <https://doi.org/10.5194/cp-18-103-2022>, 2022.
- 1073 Pedersen, J. B. T., Kroon, A., and Jakobsen, B. H.: Holocene sea-level reconstruction in the
 1074 Young Sound region, Northeast Greenland, *J. Quat. Sci.*, 26(2), 219–226, 2011.
- 1075 Rahmstorf, S., Box, J. E., Feulner, G., Mann, M. E., Robinson, A., Rutherford, S., and
 1076 Schaffernicht, E. J.: Exceptional twentieth-century slowdown in Atlantic Ocean overturning
 1077 circulation, *Nat. Clim. Chang.*, 5, 475–480, <https://doi.org/10.1038/nclimate2554>, 2015.
- 1078 Rasmussen, T. L., Pearce, C., Andresen, K. J., Nielsen, T., and Seidenkrantz, M.-S.: Northeast
 1079 Greenland: ice-free shelf edge at 79.4°N around the Last Glacial Maximum 25.5–17.5 ka,
 1080 *Boreas*, 51, 759–775, 2022.
- 1081 Reeh, N., Bøggild, C. E., and Oerter, H.: Surge of Storstrømmen, a large outlet glacier from the
 1082 Inland Ice of North-East Greenland, *Rapp. Grønlands Geol. Unders.*, 162, 201–209, 1994.
- 1083 Reilly, B. T., Stoner, J. S., Mix, A. C., Walczak, M. H., Jennings, A., Jakobsson, M., Dyke, L.,
 1084 Glueder, A., Nicholls, K., Hogan, K. A., Mayer, L. A., Hatfield, Robert, G., Albert, S., Marcott, S.,
 1085 Fallon, S., and Cheseby, M.: Holocene break-up and reestablishment of the Petermann Ice
 1086 Tongue, Northwest Greenland, *Quat. Sci. Rev.*, 218, 322–342, 2019.
- 1087 Reimer, P. J., Austin, W. E. N., Bard, E., Bayliss, A., Blackwell, P. G., Bronk Ramsey, C.,
 1088 Butzin, M., Cheng, H., Edwards, R. L., Friedrich, M., Grootes, P. M., Guilderson, T. P., Hajdas,
 1089 I., Heaton, T. J., Hogg, A. G., Hughen, K. A., Kromer, B., Manning, S. W., Muscheler, R.,
 1090 Palmer, J. G., Pearson, C., Van Der Plicht, J., Reimer, R. W., Richards, D. A., Scott, E. M.,
 1091 Southon, J. R., Turney, C. S. M., Wacker, L., Adolphi, F., Büntgen, U., Capano, M., Fahrni, S.
 1092 M., Fogtman-Schulz, A., Friedrich, R., Köhler, P., Kudsk, S., Miyake, F., Olsen, J., Reinig, F.,
 1093 Sakamoto, M., Sookdeo, A., and Talamo, S.: The IntCal20 Northern Hemisphere Radiocarbon
 1094 Age Calibration Curve (0-55 cal kBP), *Radiocarbon*, 62, 725–757,
 1095 <https://doi.org/10.1017/RDC.2020.41>, 2020.
- 1096 Rignot, E., Bjork, A., Chauche, N., and Klaucke, I.: Storstrømmen and L. Bistrup Bræ, North
 1097 Greenland, Protected From Warm Atlantic Ocean Waters, *Geophys. Res. Lett.*, 49,
 1098 <https://doi.org/10.1029/2021GL097320>, 2022.
- 1099 Rydningen, T. A., Vorren, T. O., Laberg, J. S., and Kolstad, V.: The marine-based NW
 1100 Fennoscandian ice sheet: Glacial and deglacial dynamics as reconstructed from submarine

- 1101 landforms, *Quat. Sci. Rev.*, 68, 126–141, <https://doi.org/10.1016/j.quascirev.2013.02.013>, 2013.
- 1102 Schaffer, J., von Appen, W.-J., Dodd, P. A., Hofstede, C., Mayer, C., de Steur, L., and Kanzow,
1103 T.: Warm water pathways toward Nioghalvfjerdingsfjorden Glacier, Northeast Greenland, *J.*
1104 *Geophys. Res. Ocean.*, 122, 4004–4020, <https://doi.org/10.1002/2016JC012462>. Received,
1105 2017.
- 1106 Schmidt, S., Wagner, B., Heiri, O., Klug, M., Bennike, O., and Melles, M.: Chironomids as
1107 indicators of the Holocene climatic and environmental history of two lakes in Northeast
1108 Greenland, *Boreas*, 40, 116–130, <https://doi.org/10.1111/j.1502-3885.2010.00173.x>, 2011.
- 1109 Schoof, C. G. and Clarke, G. K. C.: A model for spiral flows in basal ice and the formation of
1110 subglacial flutes based on a Reiner-Rivlin rheology for glacial ice, *J. Geophys. Res. Solid Earth*,
1111 113, 1–12, <https://doi.org/10.1029/2007JB004957>, 2008.
- 1112 Shaw, J., Pugin, A., and Young, R. R.: A meltwater origin for Antarctic shelf bedforms with
1113 special attention to megalineations, *Geomorphology*, 102, 364–375,
1114 <https://doi.org/10.1016/j.geomorph.2008.04.005>, 2008.
- 1115 Shreve, R. L.: Esker characteristics in terms of glacier physics, Katahdin esker system, Maine.,
1116 *Geol. Soc. Am. Bull.*, 96, 639–646, [https://doi.org/10.1130/0016-7606\(1985\)96<639:ECITOG>2.0.CO;2](https://doi.org/10.1130/0016-7606(1985)96<639:ECITOG>2.0.CO;2), 1985.
- 1118 Skov, D. S., Andersen, J. L., Olsen, J., Jacobsen, B. H., Knudsen, M. F., Jansen, J. D., Larsen,
1119 N. K., and Egholm, D. L.: Constraints from cosmogenic nuclides on the glaciation and erosion
1120 history of Dove Bugt, northeast Greenland, *GSA Bull.*, 1–13, 2020.
- 1121 Slabon, P., Dorschel, B., Jokat, W., Myklebust, R., Hebbeln, D., and Gebhardt, C.: Greenland
1122 ice sheet retreat history in the northeast Baffin Bay based on high-resolution bathymetry, *Quat.*
1123 *Sci. Rev.*, 154, 182–198, <https://doi.org/10.1016/j.quascirev.2016.10.022>, 2016.
- 1124 Smith, L. M. and Andrews, J. T.: Sediment characteristics in iceberg dominated fjords,
1125 Kangerlussuaq region, East Greenland, *Sediment. Geol.*, 130, 11–25,
1126 [https://doi.org/10.1016/S0037-0738\(99\)00088-3](https://doi.org/10.1016/S0037-0738(99)00088-3), 2000.
- 1127 Stacey, C. D. and Hill, P. R.: Cyclic steps on a glacial delta, Howe Sound, British Columbia,
1128 in: *Atlas of Submarine Glacial Landforms: Modern, Quaternary and Ancient*, edited by:
1129 Dowdeswell, J. A., Canals, M., Jakobsson, M., Todd, B. J., Dowdeswell, E. K. & Hogan, K. A.,
1130 Geological Society of London, 93–94, 2016.
- 1131 Stocker, T. F., Qin, D., Plattner, G.-K., Tignor, M. M. B., Allen, S. K., Boschung, J., Nauels, A.,
1132 Xia, Y., Bex, V., and Midgley, P. M.: *Climate Change 2013: The Physical Science Basis.*
1133 Contribution of Working Group I to the Fifth Assessment Report of the Intergovernmental Panel
1134 on Climate Change, Cambridge, 2013.
- 1135 Stokes, C. R. and Clark, C. D.: Geomorphological criteria for identifying Pleistocene ice
1136 streams, *Ann. Glaciol.*, 28, 67–74, <https://doi.org/10.3189/172756499781821625>, 1999.
- 1137 Stokes, C. R. and Clark, C. D.: Palaeo-ice streams, *Quat. Sci. Rev.*, 20, 1437–1457, 2001.
- 1138 Storrar, R. D., Stokes, C. R., and Evans, D. J. A.: Morphometry and pattern of a large sample
1139 (>20,000) of Canadian eskers and implications for subglacial drainage beneath ice sheets,
1140 *Quat. Sci. Rev.*, 105, 1–25, <https://doi.org/10.1016/j.quascirev.2014.09.013>, 2014.
- 1141 Syring, N., Lloyd, J. M., Stein, R., Fahl, K., Roberts, D. H., Callard, L., and O’Cofaigh, C.:
1142 Holocene interactions between glacier retreat, sea ice formation, and Atlantic water advection at

- 1143 the inner Northeast Greenland continental shelf, *Paleoceanogr. Paleoclimatology*, 35, 2020.
- 1144 Wagner, B., Bennike, O., Bos, J. A. A., Cremer, H., Lotter, A. F., and Melles, M.: A
1145 multidisciplinary study of Holocene sediment records from Hjort Sø on Store Koldewey,
1146 Northeast Greenland, *J. Paleolimnol.*, 39, 381–398, <https://doi.org/10.1007/s10933-007-9120-3>,
1147 2008.
- 1148 Weber, M. E., Niessen, F., Kuhn, G., and Wiedicke, M.: Calibration and application of marine
1149 sedimentary physical properties using a mult-sensor core logger, *Mar. Geol.*, 136, 151–172,
1150 1997.
- 1151 Weidick, A., Andreasen, C., Oerter, H., and Reeh, N.: Neoglacial glacier changes around
1152 Storstrommen, north-east Greenland, *Polarforschung*, 64, 95–108, 1994.
- 1153 Wilson, N. J. and Straneo, F.: Water exchange between the continental shelf and the cavity
1154 beneath Nioghalvfjærdsbræ (79 North Glacier), *Geophys. Res. Lett.*, 42, 7648–7654,
1155 <https://doi.org/10.1002/2015GL064944>, 2015.
- 1156 Winkelmann, D., Jokat, W., Jensen, L., and Schenke, H. W.: Submarine end moraines on the
1157 continental shelf off NE Greenland - Implications for Lateglacial dynamics, *Quat. Sci. Rev.*, 29,
1158 1069–1077, <https://doi.org/10.1016/j.quascirev.2010.02.002>, 2010.
- 1159